




REVIEW



Cite this: *J. Mater. Chem. A*, 2020, **8**, 7508

Two-dimensional transition metal carbide and nitride (MXene) derived quantum dots (QDs): synthesis, properties, applications and prospects

Binbin Shao, Zhifeng Liu, * Guangming Zeng, * Han Wang,  Qinghua Liang, Qingyun He, Min Cheng, Chengyun Zhou, Longbo Jiang and Biao Song

The progress of two-dimensional (2D) MXene-derived QDs (MQDs) is in the early stages, but the materials have aroused great interest due to their high electrical conductivity, abundant active catalytic sites, easily tunable structure, satisfactory dispersibility, remarkable optical properties, good biocompatibility, manifold functionalizations, and so on. However, up to now, there is still no review paper on MQDs. Herein, the research advances of MQDs, including their synthetic routes (top-down and bottom-up methods), properties (structural, electronic, optical and magnetic properties), functionalizations (surface modifications, heteroatom doping and the construction of composites) and applications (sensing, biomedical, catalysis, energy storage and optoelectronic devices *etc.*), are critically highlighted, and the future prospects and challenges of MQDs are discussed. This review will serve as a one-stop point for comprehending the most advanced developments of MQDs, and will hopefully enlighten researchers to employ MQDs for satisfying the growing requirements of the diverse applications.

Received 9th February 2020

Accepted 27th March 2020

DOI: 10.1039/d0ta01552k

rsc.li/materials-a

1. Introduction

So far, the resounding success of graphene materials has activated infinite passion to seek newly-fashioned 2D layered inorganic materials, such as silicene, black phosphorus (BP), transition metal dichalcogenides (TMDs), transition metal oxides (TMOs), graphitic carbon nitride (g-C₃N₄), and MXenes *etc.*, to meet new application requirements.^{1–8} In the bulk structure, these materials possess features of robust intralayer covalent bonds and weak interlayer interactions of van der Waals (vdWs). Meanwhile, their steady 2D forms (single or few-layer) could be developed and exhibit distinguishing properties to their bulk forms.^{9–11} Considering their similar 2D structure, these materials have diverse physico-chemical and optical-electrical properties, rendering them to applications in many fields.^{1,2,12–14} Compared to their 2D forms, when they are transformed to quantum dot (QD) forms (namely with a lateral size of usually <10 nm), the higher surface area and forceful quantum confinement effect *etc.* would bring more meritorious properties, and the inherent merit of the 2D counterpart will be inherited simultaneously.^{1,15,16} The emerging groups of 2D material derived QDs are provided with improved properties in comparison to their 2D counterparts, such as better dispersibility, easier functionalization, more novel luminescence,

and so on. The extraordinary and diverse properties of 2D material derived QDs enable them to be widely used in sensing, biomedical, optoelectronic device, catalysis, and energy storage applications *etc.* (Fig. 1A).^{1–3,12,17,18}

Among these 2D materials, MXenes, a new group of 2D inorganic materials, are often obtained by etching out the A layers from the MAX phase (“M” represents transition metals, “A” represents group IIIA/IVA elements and X represents C and/or N elements). MXenes possess a general formula: M_{n+1}X_nT_x ($n = 1–3$, T_x represents the surface termination groups such as –O, –F and –OH).^{20–22} Since the first report of an MXene (Ti₃C₂) in 2011,²³ dozens of MXenes, including Ti₂CT_x, Ti₃C₂T_x, Nb₂CT_x, V₂CT_x, (Ti_{0.5}, Nb_{0.5})₂C, (V_{0.5}, Cr_{0.5})₃C₂, Ti₃CNT_x and Ta₄C₃T_x *etc.*, have been reported (Fig. 1B and C).^{19,24–26} They exhibit great application potential in batteries, supercapacitors, solar cells, electromagnetic interference shielding, sensors, biomedical, optoelectronic devices and catalysis fields *etc.*, due to their excellent electrically conductive, flexibility, sensitive surface termination and environmentally friendly characteristics.^{27–36} Recently, the first example of the QDs form (Ti₃C₂) was reported, whose size could be tuned from 2.9 nm to 6.2 nm by changing the synthesis temperature.³⁷ The emergence of nanosized MQDs has aroused great interest and opens the door for further versatile theoretical and experimental studies of MQDs in the near future. Like other QDs, the MQDs exhibit multifarious fascinating properties, including natural hydrophilicity, satisfactory biocompatibility, ready functionalization, and excellent photoluminescence (PL) properties, because of their size and quantum confinement effects, and the unrivalled properties

College of Environmental Science and Engineering, Hunan University, Key Laboratory of Environmental Biology and Pollution Control (Hunan University), Ministry of Education, Changsha 410082, P. R. China. E-mail: zhifengliu@hnu.edu.cn; zgming@hnu.edu.cn

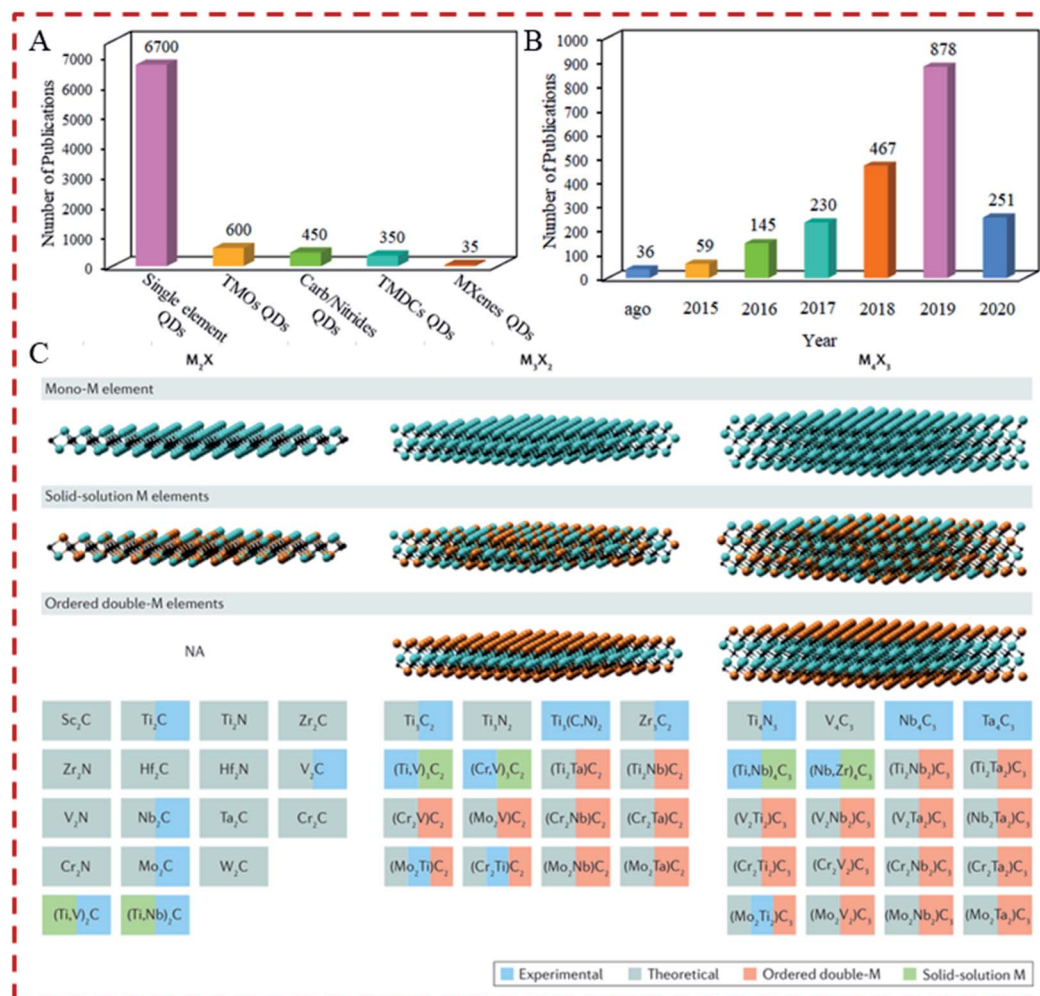


Fig. 1 (A) Number of journal publications on typical 2D material derived QDs ("Single element QDs" represent graphene, phosphorene, silicene, germanene and carbon QDs; "TMOs QDs" represent ZnO , WO_3 and MoO_3 QDs; "Carb/Nitride QDs" represent SiC , $\text{g-C}_3\text{N}_4$ and h-BN QDs; "TMDCs QDs" represent MoS_2 , WS_2 , MoSe_2 and WSe_2 QDs) (Source: Web of Science, 2015s to 2020s). (B) Number of journal publications on MXenes (Source: Web of Science, Keyword: MXenes). (C) MXenes reported so far. MXenes can have at least three different formulas: M_2X , M_3X_2 and M_4X_3 . They can be made in three different forms: mono-M elements (e.g. Ti_2C); a solid solution of at least two different M elements (e.g. $(\text{Ti}, \text{V})_3\text{C}_2$); ordered double-M elements, in which one transition metal occupies the perimeter layers and another fills the central M layers (e.g. Mo_2TiC_2 , in which the outer M layers are Mo and the central M layers are Ti). Solid solutions on the X site produce carbonitrides.¹⁹ Copyright 2017 Nature Reviews Materials.

immediately expand their applications to optoelectronic, biological, catalysis, and energy areas *etc.*^{1,3,38–41}

To date there have only been a small number of research articles and high-quality review papers regarding 2D MXenes,^{13,42–45} and the research on MQDs is increasing. Therefore, it is necessary to write a review paper of MQDs, which could provide a crucial role in guiding the future research of MQDs. Herein, we aim to summarize the updated research advances and provide critical insights into the booming topic of "MQDs". In this review, the synthetic techniques, unique properties, and extensive applications of MQDs are summarized, and the challenges and future prospects in this field are briefly discussed (Fig. 2). This review will contribute to the unfolding and will guide new research directions of MQDs to satisfy the high requirements in diverse applications.

2. Synthesis of MQDs

Synthesis methods for QDs have been extensively developed over the past decade. Generally, the strategies include two groups: top-down and bottom-up methods. By varying the synthetic method, we can adjust their size, control their morphology and structure, as well as functionalize them, rendering satisfactory structures and properties of the prepared QDs.^{1,2} MQDs are an important part of QDs, and the above synthesis strategies can also be suitable for MQDs; the reported syntheses of MQDs are summarized as follows (Table 1).

2.1. Top-down methods

In the top-down methods, QDs (e.g. graphene, $\text{g-C}_3\text{N}_4$, BP, MoS_2 *etc.*) are usually synthesized *via* the cleavage of relatively large

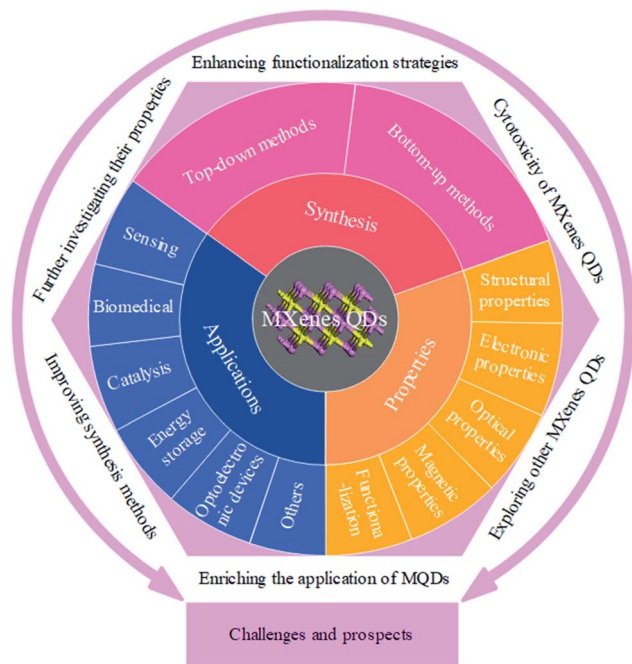


Fig. 2 An overview of synthesis, properties and applications of MXene QDs.

bulk precursors by chemical, electrochemical (EC), or physical methods.^{74–77} For most top-down methods, oxygen-containing functional groups were first established on 2D nanosheets, upon which defects could be created. The defects could then serve as chemically reactive sites, allowing a layered structure to be cut into smaller structures, and finally into QDs.^{1,78} The top-down methods have the superiorities of simple operation, the use of abundant raw materials, and large-scale production. However, they are also limited in some shortcomings, such as a low production yield and the requirement for special treatments.^{1,2,12}

Up to now, the top-down methods have been widely used to obtain MQDs (most of them are Ti_3C_2 QDs). According to the different synthesis conditions, the “top-down methods” mainly include hydrothermal/solvothermal, ultrasonic, ball-milling, intercalation and combined methods.^{37,38,41,46–48,63} Among these methods, the hydrothermal method is the most common method, using the 2D MXenes as precursors.^{3,20,37,39,40,49,51,56–58,65} Generally, the hydrothermal reaction temperature (HRT) is greatest at 100–150 °C, and the reactants are in neutral or slightly alkaline or slightly acidic environments (pH = 6–9). The reaction time depends on the HRT and the pH, and usually the higher HRT and pH leads to a shorter reaction time. Furthermore, the size, morphology and properties of MQDs can also be adjusted by changing these reaction conditions. For instance, Xue *et al.*³⁷ first reported that the Ti_3C_2 QDs could be prepared by a hydrothermal method (Fig. 3A). The colloidal Ti_3C_2 QDs with different sizes could be obtained through adjusting the hydrothermal temperature, where the average lateral sizes (ALS) of the Ti_3C_2 QDs were 2.9, 3.7, and 6.2 nm, and the average thicknesses (AT) were 0.99, 0.91, and 0.89 nm, at 100 °C, 120 °C,

and 150 °C, respectively. These results revealed that the majority of Ti_3C_2 QDs were monolayers. Meanwhile, at a relatively low reaction temperature (100 °C), the Ti_3C_2 QDs showed the original structure of MXene, and this could be confirmed according to the lattice spacing of 0.266 nm assigned to the (0110) plane of Ti_3C_2 MXene. However, when the reaction temperature was 150 °C, a number of the Ti atoms were drawn out and an amorphous structure appeared (Fig. 3B–G). Since then, more Ti_3C_2 QDs have been prepared under different hydrothermal conditions.^{39,40,49,51,58,65} Furthermore, the heteroatom-doped Ti_3C_2 QDs, including N- Ti_3C_2 QDs, P- Ti_3C_2 QDs, S- Ti_3C_2 QDs, P, N- Ti_3C_2 QDs and S, N- Ti_3C_2 QDs,^{3,56,57} have also been synthesized *via* a hydrothermal method by adding the corresponding precursor of the elements in the reaction system. All these heteroatom-doped Ti_3C_2 QDs displayed an ultra-small size, and exhibited better performance in various applications. Except for Ti_3C_2 QDs, Cao *et al.*²⁰ also reported that the V_2C QDs could be prepared *via* the hydrothermal method (pH = 9, 160 °C for 10 h) using the V_2C nanosheets as a precursor. The V_2C QDs exhibited ALS and AT values of 16 and 0.8 nm, respectively, indicating that a majority of the V_2C QDs were monolayers.

Similar to the hydrothermal method, the solvothermal method has also been used to synthesize MQDs. Instead of using water as the reaction medium, as in the hydrothermal method, organic solvents such as ethanol, dimethylformamide (DMF) and dimethyl sulfoxide (DMSO), were used as the reaction medium in the solvothermal method. Compared to the hydrothermal method, the solvothermal method could better control the size, dispersion and morphology of MQDs.^{41,79,80} Xu *et al.*⁴¹ utilized Ti_3C_2 MXene as the precursor to prepare three Ti_3C_2 QDs by the solvothermal method, namely e- Ti_3C_2 QDs, f- Ti_3C_2 QDs and s- Ti_3C_2 QDs, using ethanol, DMF and DMSO as the solvent, respectively (Fig. 3H). The results showed that all supernatants exhibited good dispersion, stability and different colors (Fig. 3I), and all of them were derived from the Ti_3C_2 MXene according to their matched lattice parameters. Meanwhile, the sizes of the MQDs were significantly dependent on the solvents, their ALS values were 1.8 ± 0.1 , 2.5 ± 0.2 , and 3.3 ± 0.2 nm for s- Ti_3C_2 QDs, e- Ti_3C_2 QDs, and f- Ti_3C_2 QDs, respectively, and their AT values were in the range of 1.0–2.5 nm, indicating that these Ti_3C_2 QDs were few-layered. Their different sizes could be as a result of the co-action of the polarity, boiling point, and oxidation degree of the solvents.^{81,82}

Compared to the simple hydrothermal/solvothermal methods, combining ultrasound and hydrothermal/solvothermal methods could be the most effective strategies,^{38,47,62,72} since ultrasonication can cause acoustic cavitation and shockwaves in a “good solvent”. Meanwhile, it is beneficial for degassing to suppress the oxidation of MXenes, resulting in delaminating and accelerating the fragmentation of 2D MXenes to QDs.^{83,84} In general, two ultrasonic means are frequently employed, namely probe ultrasonic and bath ultrasonic methods. The probe ultrasonic method exhibits the larger crushing strength, where the obtained materials are more dispersed and finer in comparison to the bath ultrasonic method. However, the operation of an ultrasonic probe requires

Table 1 Recent studies of MQDs^a

MQDs	Synthesis methods	Functionalization	Size	Applications	Ref.
Ti ₃ C ₂	TDM: hydrothermal (pH = 9.0, 100 °C, 120 °C or 150 °C for 6 h)	SM: -OH, -O, -F, -NH	ALS: 2.9, 3.7, 6.2 nm; AT: 0.99, 0.91, 0.89 nm, under 100 °C, 120 °C, 150 °C respectively	Bioimaging; Zn ²⁺ detection	37
	TDM: ultrasound (probe ultrasonic (480 W, 6 h), bath ultrasonic (300 W, 10 h))	SM: -OH, -O, Al(OH) ₄ ⁻ , PEG	ALS: 4.9 ± 0.6 nm; AT: 1.2 ± 0.3 nm	Bioimaging; photothermal therapy	46
	TDM: ultrasound-solvothermal (DMF, bath ultrasonic (700 W, 3 h), 200 °C for 2 h)	SM: -OH, -O, -F	ALS: 4–10 nm; AT: 0.68–2.74 nm	Fluorescent ink; light-emitting diodes; bioimaging	47
	TDM: ball-milling (with C, S, P or Si, 48 h at 550 rpm)	SM: -OH, -O, -F; composite: Ti ₃ C ₂ QDs/C or S or P or Si	ALS: 175, 19.2, 6.2, 2.7 nm; AT: 44, 4.5, 3.7, 0.9 nm, for ball-milling with C, S, P, Si, respectively	Sodium-ion battery	48
	TDM: hydrothermal (pH = 7, 120 °C for 24 h)	SM: -OH, -O, -F, PEI	ALS: 10.2 ± 0.5 nm; AT: 1.0 nm	Bioimaging; pH sensor	49
	TDM: hydrothermal (pH = 7, 120 °C for 12 h)	SM: -OH, -O, -F, PEI	ALS: 3–6 nm	H ₂ production	50
	TDM: hydrothermal (pH = 9, 100 °C for 6 h)	SM: -OH, -O, -F, -NH	ALS: 4.2 ± 0.6 nm; AT: 1.2 and 2.0 nm	Enzyme assay; cell identification	51
	TDM: hydrothermal (pH = 7, 100 °C for 24 h)	SM: -OH, -O, -F, PLL	ALS: 3 nm	Cytochrome c and trypsin detection	52
	TDM: reflux (6 M HNO ₃ , refluxed at 120 °C for 8–72 h)	SM: -OH, -O, -F, PEI	ALS: 10 nm; AT: 1.0 nm	Glutathione detection	53
	TDM: reflux (2.5% TMAOH, refluxed at 110 °C for one day)	SM: -OH, -O, -F	ALS: 3–4.8 nm	—	54
	TDM: solvothermal (DMF, 150 °C for 8 h)	Doping: N-doping	ALS: 6.2 nm; AT: 1.0 nm	Cu ²⁺ detection	55
	TDM: solvothermal (ethanol, DMF or DMSO, 120 °C for 6 h)	SM: -OH, -O, -F	ALS: 1.8 ± 0.1, 2.5 ± 0.2, 3.3 ± 0.2 nm, for DMSO, ethanol, DMF, respectively; AT: 1.0–2.5 nm	Fe ³⁺ detection; fluorescent staining	41
	TDM: hydrothermal (pH = 7, 120 °C, 160 °C or 200 °C for 12 h)	SM: -OH, -O, -F; doping: N-doping	ALS: 3.93, 3.7, 5.76 nm; AT: 0.7, 1.4, 3.8 nm under 120 °C, 160 °C, 200 °C, respectively	Fe ³⁺ detection; H ₂ O ₂ detection	56
	TDM: hydrothermal (pH = 7, 120 °C for 12 h)	SM: -OH, -O, -F; doping: P-doping, N-doping, P, N-codoping	ALS: 2.73 ± 0.50, 3.14 ± 0.50, 2.97 ± 0.50 nm; AT: 0.85 ± 0.02, 0.93 ± 0.05, 0.71 ± 0.03 nm, for P, N-codoping, N-codoping, P-codoping, respectively	Bioimaging; Cu ²⁺ detection	57
	TDM: hydrothermal (pH = 7, 100 °C for 2 h)	SM: -OH, -O, -F; composite: Ti ₃ C ₂ QDs/Ti ₃ C ₂ nanosheets/S	ALS: 2.5 nm	Lithium-sulfur battery	39
	TDM: hydrothermal (pH = 7, 150 °C for 12 h)	SM: -OH, -O, -F; doping: S-doping, N-doping, S, N-codoping	ALS: 50, 15–35, 9–13 nm; AT: 20.41 and 14.15, 8.67, 25.2 nm, for S, N-codoping, N-codoping, S-codoping, respectively	Light-emitting diodes	3
	TDM: hydrothermal (pH = 6, 100 °C for 6 h)	SM: -OH, -O, -F	ALS: 2 nm	Methanol oxidation reaction; oxygen reduction reaction	58
	TDM: hydrothermal (pH = 8, 120 °C for 12 h)	SM: -OH, -O, -F, GSH	ALS: 2.5 nm	Uric acid detection	59
	TDM: hydrothermal (pH = 9, 100 °C for 6 h)	SM: -OH, -O, -F; composite: Co-Ti ₃ C ₂ QDs	ALS: 3.48, 5.43, 6.66, 7.28 nm	Water oxidation	60
			ALS: 3.0 nm; AT: 1.98 nm	Nonvolatile memory devices	61

Table 1 (Contd.)

MQDs	Synthesis methods	Functionalization	Size	Applications	Ref.
	TDM: hydrothermal (pH = 8, 100 °C for 6 h)	SM: -OH, -O, -F; composite: ITO/Ti ₃ C ₂ T _x QDs-PVP/Au			
	TDM: ultrasound-hydrothermal (probe ultrasonic (120 W, 6 h), bath ultrasonic (300 W, 10 h), 120 °C for overnight)	SM: -OH, -O, -F, PEI; composite: Ti ₃ C ₂ T _x QDs/Cu ₂ O nanowires	ALS: 1–7 nm; AT: 1–1.2 nm	CO ₂ reduction	38
	TDM: hydrothermal (pH = 9, 130 °C for 6 h)	SM: -OH, -O, -F, -NH	ALS: 4 nm	Immunomodulation	40
	TDM: ultrasound-hydrothermal (ultrasonic (600 W, 6 h), 80 °C for 48 h)	SM: -OH, -O, -F, -NH	ALS: 13.1 nm; AT: 1.362 nm	Light-emitting diodes	62
	TDM: intercalation-ultrasound (25% TMAOH, bath ultrasonic for 10 h)	SM: -OH, -O, -F	ALS: 1–7 nm	Ag ⁺ , Mn ²⁺ detection	63
	TDM: intercalation-ultrasound (25% TMAOH, tip ultrasonic for 6 h)	SM: -OH, -O, -F; composite: Ti ₃ C ₂ T _x nanosheets/Ti ₃ C ₂ T _x QDs/RGO fibers	ALS: 3.2 nm	Supercapacitor	64
	TDM: hydrothermal (pH = 7, 120 °C for 4 h)	SM: -OH, -O, -F, PEI; composite: Ti ₃ C ₂ QDs/TiO ₂	ALS: 8.2 nm; AT: 1.02 nm	Glutathione detection	65
	TDM: intercalation-ultrasound (25% TMAOH, bath ultrasonic (200 W, 20 h))	SM: -OH, -O, -F; composite: Ti ₃ C ₂ QDs-encapsulated liposomes	ALS: 3.4 nm; AT: 1.65 nm	Prostate-specific antigen detection	66
	TDM: intercalation-ultrasound (25% TMAOH, bath ultrasonic for 10 h)	SM: -OH, -O, -F	ALS: 4 nm; AT: 1 nm	—	67
	TDM: intercalation-ultrasound (DMSO, bath ultrasonic for 10 h)	SM: -OH, -O, -F	ALS: 1.75 ± 0.43 nm; AT: 1.2 nm	Fe ³⁺ detection	68
Mo ₂ C	TDM: ultrasound (bath ultrasonic (400 W, 20 h) at room temperature)	SM: -OH, -O	ALS: 6 nm; AT: 1–1.5 nm	Bioimaging; photothermal therapy	69
	BUM: molten salt (molybdenum acetylacetonate, NaCl, 800 °C for 2 h)	Composite: Mo ₂ C QDs/carbon nanosheets	ALS: 2–3 nm	Nitrogen reduction reaction	70
	BUM: pyrolysis (molybdic acid, 700 °C for 2 h)	Composite: Mo ₂ C QDs/carbon polyhedrons	ALS: 4.5 nm	Microwave absorption	71
V ₂ C	TDM: hydrothermal (pH = 9, 160 °C for 10 h)	SM: -OH, -O, -F, PEG, TAT peptide	ALS: 16 nm; AT: 0.8 nm	Bioimaging; photothermal therapy	20
	TDM: ultrasound-hydrothermal (ultrasonic 1 h, alkaline, 120 °C for 2 h)	SM: -OH, -O, -F, -NH	ALS: 4.13 nm; AT: 2–3 nm	Light-emitting diodes	72
Ti ₂ C	TDM: intercalation-ultrasound (25% TMAOH, bath ultrasonic for 10 h)	SM: -OH, -O, -F	ALS: 2–5 nm	—	67
Nb ₂ C	TDM: intercalation-ultrasound (25% TPAOH, pulsed ultrasonic for 10 h)	SM: -OH, -O, -F	ALS: 1–5 nm; AT: 1.2 nm	Fe ³⁺ detection; bioimaging	73

^a TDM: top-down method; BUM: bottom-up method; SM: surface modification; ALS: average lateral size; AT: average thickness; DMF: dimethylformamide; TMAOH: tetramethylammonium hydroxide; TPAOH: tetrapropylammonium hydroxide; DMSO: dimethyl sulfoxide; PEG: polyethylene glycol; PEI: polyethylenimine; PLL: ε-poly-L-lysine; GSH: glutathione; ITO: indium tin oxide; PVP: polyvinylpyrrolidone; RGO: reduced graphene oxide.

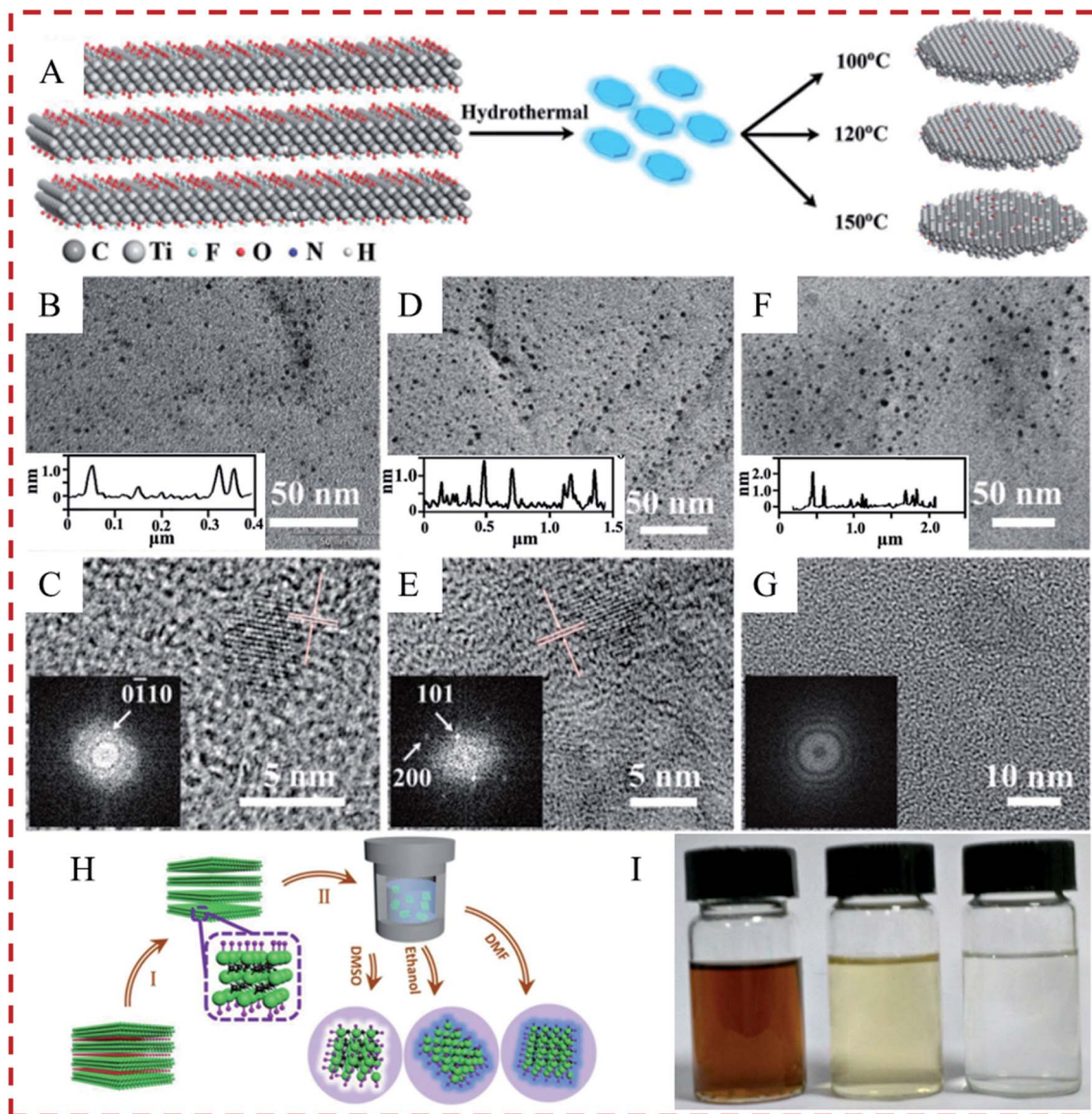


Fig. 3 (A) Schematic diagram of preparation of Ti₃C₂ QDs by a hydrothermal method.³⁷ Copyright 2017 Advanced Materials. TEM, HRTEM, and AFM images of Ti₃C₂ QDs-100 (B and C), Ti₃C₂ QDs-120 (D and E) and Ti₃C₂ QDs-150 (F and G).³⁷ Copyright 2017 Advanced Materials. (H) Schematic for the preparation of Ti₃C₂ QDs by the solvothermal method in different solvents of DMF, DMSO, or ethanol, respectively.⁴¹ Copyright 2018 Advanced Optical Materials. (I) Color contrast picture of different Ti₃C₂ QD solutions, left to right represent s-MQDs, f-MQDs, and e-MQDs, respectively.⁴¹ Copyright 2018 Advanced Optical Materials.

more cautious attention.⁸⁵ Zeng *et al.*³⁸ employed the ultrasound-hydrothermal method to prepare Ti₃C₂ QDs. In detail, the dispersion of the Ti₃C₂ sheet precursor was first performed by two stages of ultrasound, including a tip sonication (120 W) for 6 h in an Ar atmosphere and subsequent bath sonication (300 W) for 10 h. Afterwards, the dispersion was hydrothermally treated at 120 °C overnight. Zhou *et al.*⁴⁷ developed Ti₃C₂-derived graphene QDs (GQDs) by the ultrasound-solvothermal method. The results showed that the product yield of GQDs reached as high as 32.6%. Furthermore, the V₂C QDs have also been well prepared *via* the ultrasound-hydrothermal method.⁷²

In addition to the above synthesis strategies, some other top-down approaches could be introduced to prepare MQDs, such as direct ultrasound, ball-milling, intercalation *etc.*^{46,48,54,63,66,67,69} For example, ultra-small Ti₃C₂ QDs (ALS: 4.9 nm, AT: 1.2 nm) have been synthesized *via* a two-step ultrasound strategy (probe sonication at 480 W for 6 h) to break the bulk into smaller sizes in order to expose the fresh edges and surfaces. Subsequent bath sonication (300 W, 10 h) was used to split the Ti₃C₂ nanosheets in 28.6% tetrabutylammonium hydroxide (TBAOH) aqueous solution using the bulk Ti₃AlC₂ as a precursor (Fig. 4A).⁴⁶ Similarly, the Ti₃C₂ QDs and Ti₂C QDs have also been prepared by the intercalation-ultrasound method, namely that the MXene nanosheet precursors were first reacted in 25%

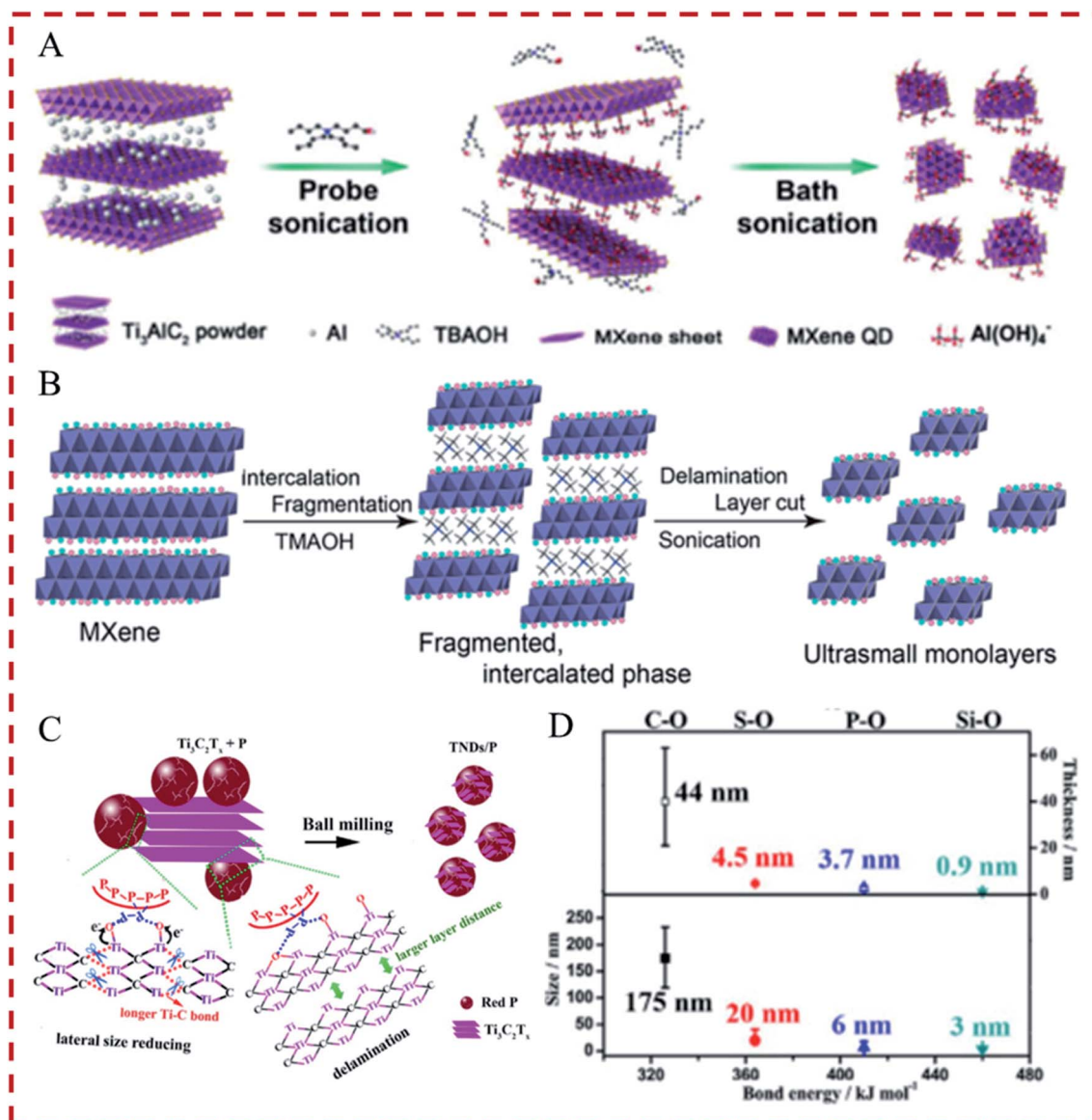


Fig. 4 (A) Schematic showing the preparation of Ti_3C_2 QDs by a two-step ultrasound strategy.⁴⁶ Copyright 2017 Nanoscale. (B) Schematic illustration for preparing Ti_3C_2 or Ti_2C QDs by the intercalation-ultrasound method.⁶⁷ Copyright 2017 ACS Nano. (C) Schematic illustration of the formation of Ti_3C_2 QDs by ball-milling with solid-state element (carbon, sulfur, red phosphorus or silicon) assistance.⁴⁸ Copyright 2018 ChemNanoMat. (D) The size and thickness distributions of Ti_3C_2 QDs after ball-milling.⁴⁸ Copyright 2018 ChemNanoMat.

tetramethylammonium hydroxide (TMAOH) aqueous solution for 24 h. Subsequently, the intercalated-MXenes were treated in an ultrasonic bath for 10 h to obtain Ti_3C_2 or Ti_2C QDs (Fig. 4B).^{66,67} In addition, the Mo_2C QDs have also been prepared through a simpler one-step bath ultrasonic treatment (400 W, 2 h, room temperature) using Mo_2C powder as a precursor.⁶⁹ Furthermore, it has also been reported that the Ti_3C_2 QDs can be obtained by reflux method, namely the prepared TMAOH intercalated multilayered Ti_3C_2 was thermally refluxed in 2.5% TMAOH for 24 h at 110°C .⁵⁴ The obtained Ti_3C_2 QDs with high yields ($\sim 60\%$) have good dispersibility (3–4.8 nm). In addition, the Ti_3C_2 QDs can also be constructed by the ball-milling method. Zhang *et al.*⁴⁸ found that Ti_3C_2 QDs with different sizes were formed when ball-milling Ti_3C_2 MXene with different

solid-state elements (carbon, sulfur, red phosphorus or silicon) under an Ar shield (Fig. 4C). However, it is difficult to remove solid-state elements from the final products due to the formation of Ti–O–P (or C, or S, or Si) bonds, and hence this method is more suitable for synthesizing composite materials (Fig. 4D). Although the operation of the above method is relatively simple, the satisfactory MQDs can also be obtained, as long as the preparation conditions are well controlled, therefore research on simpler synthesis methods should be encouraged.

Although the above top-down methods are effective for obtaining MQDs, they still have some disadvantages, such as time consumption, low production yield, and low repeatability. Thus more effort should be paid into investigating more superior synthesis methods, such as electrochemical methods, alkali

metal (e.g. Li or K) intercalation, microwave irradiation, and so on, and these methods have been widely studied in the synthesis of other QD materials, possessing the advantages of simple operation, eco-friendliness, low cost, good reproducibility, and easy large-scale preparation *etc.*^{1,12,86,87}

2.2. Bottom-up methods

Compared to the top-down methods using the bulk materials as precursors, the bottom-up methods employ the molecular materials as precursors.^{1,88} The MQDs could also be synthesized from small organic and inorganic molecular precursors *via* bottom-up methods. Bottom-up methods possess some virtues, such as sufficient atomic utilization, better structure and morphology control, and easier functionalization *etc.*, endowing the QDs with better configurations and properties.^{2,70,71}

Recently, Cheng *et al.*⁷⁰ obtained a Mo₂C QDs/carbon nanosheet (Mo₂C/C) composite *via* a molten salt synthesis strategy (Fig. 5A). In summary, the molybdenum acetylacetonate precursor, sucrose and NaCl were mixed evenly. Afterwards, the mixture was calcinated at 800 °C for 2 h under Ar protection. TEM and HRTEM images showed that the size of the Mo₂C QDs was about 2–3 nm, the interplanar spacing was about 2.37 Å, which corresponded with the (002) plane of Mo₂C. Wang *et al.*⁷¹

employed a pyrolysis method to synthesize a Mo₂C QDs/carbon polyhedron composite (Fig. 5B). In detail, Mo/ZIF-8 was prepared first using molybdic acid, zinc acetate and 2-methylimidazole as precursors, then Mo/ZIF-8 was pyrolyzed at 700 °C for 2 h in an Ar atmosphere. Finally, the zinc species was removed by acidic etching. The formed Mo₂C QDs showed an ALS of 4.5 nm, and their lattice spacing (0.24 nm) matched well with the (111) plane of cubic-Mo₂C.

The above studies provide a good basis for the preparation of MQDs by bottom-up methods, but simple, efficient and low-toxicity precursors, mild reaction conditions, good crystallinity and monodispersity, as well as high yields for large-scale production still need to be considered. Meanwhile, due to the relatively simple operation in comparison to top-down methods, the one-pot bottom-up methods are supposed to prepare MQDs in order to meet requirements of incremental applications in the future. Therefore, although there is limited research on bottom-up methods for the synthesis of MQDs, the research is promising and more attention should be paid on these strategies.

3. Properties of MQDs

The 2D MXenes possess many excellent properties. Therefore, MQDs will not only inherit the excellent properties of 2D

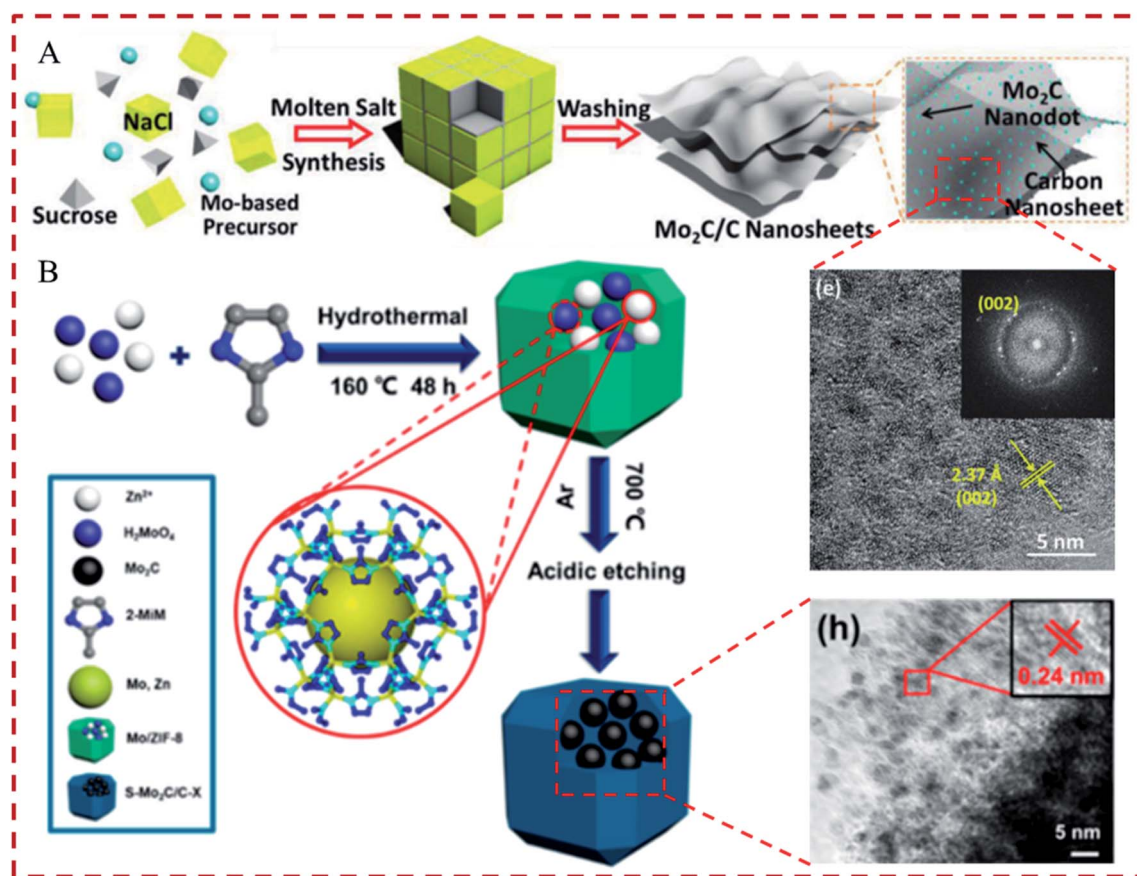


Fig. 5 (A) Schematic illustration of the molten salt synthesis route for Mo₂C QDs/C nanosheets and the corresponding TEM image.⁷⁰ Copyright 2018 Advanced Materials. (B) Schematic illustration of preparing Mo₂C QDs-decorated carbon polyhedrons by the pyrolysis method and the corresponding TEM image.⁷¹ Copyright 2018 ACS Applied Nano Materials.

MXenes, but they will also exhibit unique properties due to quantum size effects.^{1,2} In this review, the structural, electronic, optical, and magnetic properties, as well as the functionalization, of MQDs have been summarized and discussed.

3.1. Structural properties

The research on the structure of MQDs is of great significance for comprehending their properties. Typically, the MXenes were prepared by etching out the “A” element of the MAX phases, and this could be confirmed by the XRD pattern (Fig. 6A). The difference between 2D MXenes and MQDs lies in the different sizes, where the MQDs exhibit single or fewer layers in thickness and the diameter is usually less than 10 nm.^{37,41} Meanwhile, since the MAX phases have hexagonal symmetry, the derived MQD systems form hexagonal lattices with the same symmetry, as shown in Fig. 6B.⁶⁹ Moreover, the $M_{n+1}X_n$ MXenes consist of $2n+1$ layers, where the “X” layer is clamped by two “M” layers, and the topological height of a single MXene stack is generally <1 nm.²⁵ Furthermore, the coordination amount of a transition metal ion is usual six, so it is natural to assume that the transition metals in MXenes make six chemical bonds with the neighboring X atoms.^{43,89}

Additionally, in all practical cases, MQDs are terminated with surface groups (e.g. $-F$, $-OH$ and $-O$) resulting from the etching of the MAX phase. For instance, Qin *et al.*⁵⁴ fabricated Ti_3C_2 QDs by the top-down method, and their XPS and FTIR

spectra both indicated the existence of $-F$, $-OH$, and $-O$ groups (Fig. 6C and D). Furthermore, O - and OH -terminated MXenes were considered to be more stable, due to the fact that $-F$ termination is easily superseded by $-OH$ when washed and/or stored in water.^{90,91} Meanwhile, previous studies also showed that the $-OH$ group could be transformed into $-O$ termination at high temperatures and/or in the metal adsorption process.⁹² As shown in Fig. 6E and F, the OH group decreases and the O element increases with the increase of synthesis temperature.³⁷ O -terminated MXenes can further convert to bare MXenes after contact with Mg , Ca , and Al metals *etc.*⁹² Previous forecasts suggested that the terminated groups stand a good chance of being located above the hollow positions between three adjacent C atoms. Nevertheless, recent research has indicated that the positions of the terminated groups are more complex than predicted. Three feasible positions for these surface groups have been put forward: (a) located on the roof of “M” atoms, (b) at hollow position I between three adjacent “X” atoms below the “M” atoms, and (c) at hollow position II on roof of the “X” atoms. The density functional theory (DFT) calculation found that the terminated groups situated at position I on the two sides of the MXenes should be the most stable form for most MXenes, because of less steric hindrance. However, position II would be better for MXenes, when the “M” atoms cannot offer enough electrons (e^-) for both “X” atoms and surface groups. In particular, O -termination requires two e^- to consolidate its

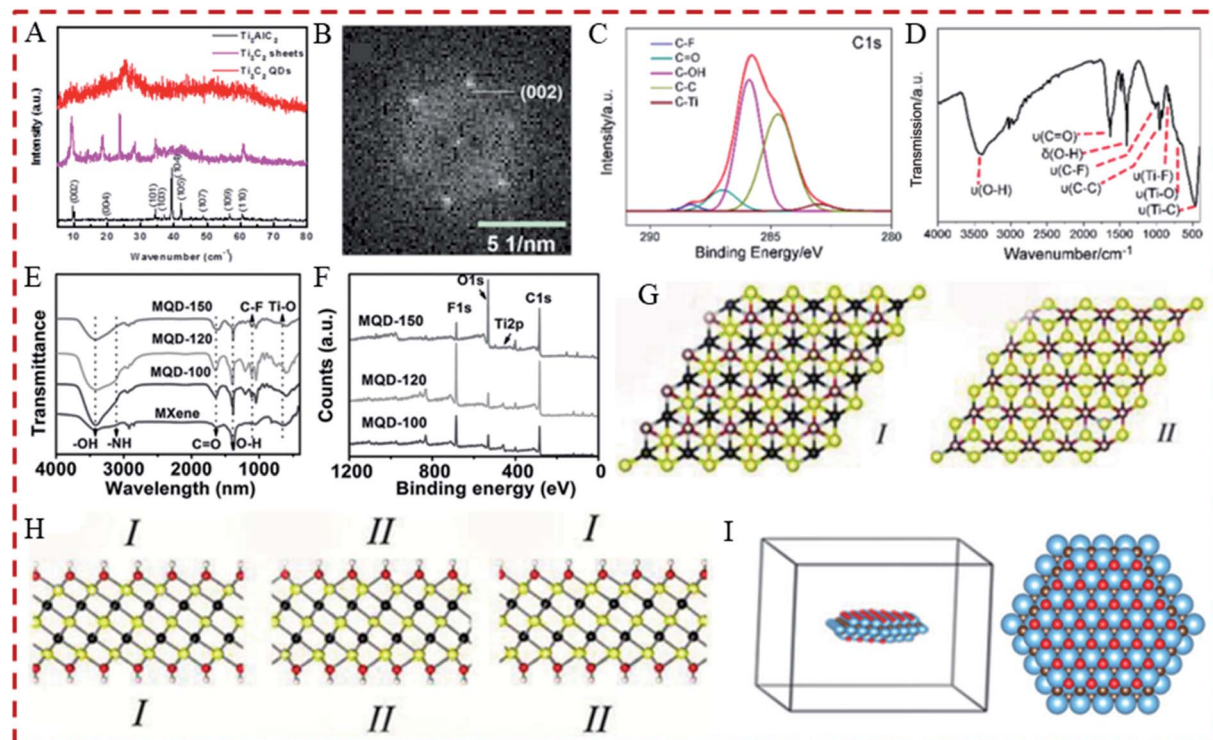


Fig. 6 (A) XRD patterns of Ti_3AlC_2 , Ti_3C_2 nanosheets and Ti_3C_2 QDs.³⁸ Copyright 2019 Advanced Functional Materials. (B) The FFT pattern of Mo_2C QDs.⁶⁹ Copyright 2018 Materials. (C and D) XPS spectrum of C 1s and the FTIR spectrum of the obtained Ti_3C_2 QDs.⁵⁴ Copyright 2018 Nanoscale. (E and F) FTIR and XPS spectra of the as-synthesized Ti_3C_2 QDs.³⁷ Copyright 2017 Advanced Materials. (G and H) Side and top views of $M_3X_2(OH)_2$.⁹³ Copyright 2018 Advanced Materials. (I) The side and top views of the O-terminated Ti_3C_2 QDs model.³⁸ Copyright 2019 Advanced Functional Materials.

adsorption site, and this differs from OH[−] and F-terminations, which just need one e[−] from the “M” atoms. As a result, O-termination on MXenes with low valence “M” atoms are inclined to be located at position II or in a mixture of position I and II (Fig. 6G and H).^{89,93,94} The accurate position of the terminated groups depends on both their type and the composition of the MXenes, and this requires further investigation.

Notably, MXenes are frequently modeled with consistent terminated types, which is unrealistic. In order to more precisely present the complex structure of the MXenes system, further modeling is needed to adapt to the coexistence and random adsorption of multifarious terminated groups in MXenes. Meanwhile, interlayer interactions, such as vdW's forces, hydrogen bonding *etc.*, should also be considered, due to the frequent occurrence of stacking.^{42,92,94–98} Compared to the 2D MXenes, the model of MQDs could be constructed in a more precise way due to the finite thickness of MQDs, thus their properties can be predicted more accurately using DFT calculations. For example, Zeng *et al.*³⁸ built the Ti₃C₂ QDs model of a hexagonal cluster with a diameter of 24.3 Å for a DFT calculation (Fig. 6K), where the size of the model was close to that of the experiment, and so the results of DFT calculations will be more reliable.

3.2. Electronic properties

The electronic properties of MXenes are of great importance. As for the MQDs, their electronic properties should be more attractive due to their small-size effect. In principle, the MQDs have metallic conductivity with high electron density close to the Fermi level (E_F), because of d-e[−] from the “M” atoms.⁸⁹ Experiments have shown that the electric conductivities of MXene sheets are analogous to multilayered graphene (resistance in the range of 22–339 Ω) and are higher than those of carbon nanotubes and reduced graphene oxide materials.^{36,98} However, the electronic conductivity is adjustable according to the composition and terminated groups of MQDs, and it has been discovered that the resistance is enhanced by the number of layers and the existence of surface groups, thus the nanosized MQDs will be better for electron transfer in comparison to their stacked counterparts.^{98,99} Meanwhile, in a well-organized double-“M” form, it must be emphasized that the outer “M” layers have more effect on the electronic properties than the inner “M” layer.¹⁰⁰ For instance, Zhang *et al.*^{39,48} applied Ti₃C₂ QDs to elevate the performance of a lithium–sulfur battery. Zeng *et al.*^{38,58,70} also verified that the activity of photo/electrocatalysts can be improved by MQDs (Ti₃C₂ QDs and Mo₂C QDs). The improved performance could be due to the excellent electrical conductivity of MQDs, which dramatically facilitates the charge transfer and provides more active sites (Fig. 7A–C). Furthermore, it should be emphasized that the MXene nitrides and carbonitrides possess higher density of states (DOS) overall than MXene carbides, and this could be due to the more robust “M”–N bond (in comparison to “M”–C bond) and the additional nitrogen electron, thus resulting in superior electrical conductivity.⁹⁸

The energy band structure (EBS) and DOS of MXenes have been widely investigated through DFT calculations. The EBS was drawn along the high symmetry points of the hexagonal BZ, and the DOS was projected on the “M”-d and “X”-p states.⁹⁹ It should be highlighted that the terminated groups could significantly alter the electronic properties, and this could result from the formation of new bands below E_F , and so E_F would decrease, thus dramatically reducing the DOS, raising the d band up above E_F and generating an energy gap (E_g),^{93,98} especially for O-terminated MXenes such as Ti₂CO₂, Zr₂CO₂, Hf₂CO₂, Sc₂CF₂, Sc₂C(OH)₂, and Sc₂CO₂ with E_g values of 0.24, 0.88, 1.0, 1.03, 0.45, and 1.8 eV, respectively. Among these MXenes, apart from Sc₂C(OH)₂ that is calculated as a direct band-gap semiconductor, all others are recognized as indirect band-gap semiconductors.¹⁰¹ This occurs because of the hybridization between the p-orbital of surface terminations and the d-orbital of “M” atoms. Additionally, the work function (WF) of MXenes was also predicted by DFT. Generally, the rank of WF follows: O- > F- ≥ bare > OH-terminated MXenes, owing to the surface terminations that cause the E_F to shift lower, thus enhancing the WF of O- and F-terminated MXenes.^{93,102} Xu *et al.*⁵⁶ employed DFT calculations to investigate the DOS of both pristine Ti₃C₂O₂ QDs and N-Ti₃C₂O₂ QDs. For pristine Ti₃C₂O₂ QDs, both E_g and a sub-gap (S_g) exist, however, for N-Ti₃C₂O₂ QDs, the E_g broadens and incorporates the gap states in the S_g , as shown in Fig. 7D. Zeng *et al.*³⁸ also calculated the DOS and Fermi levels of O-terminated Ti₃C₂ QDs. The results indicated that O-terminated Ti₃C₂ QDs exhibit plentiful electronic states across the E_F , revealing the distinguished conductivity of O-terminated Ti₃C₂ QDs (Fig. 7E and F).

Furthermore, a few MXenes are identified as 2D topological insulators (TIs).^{103,104} In such materials, the opposite spin e[−] will travel in the opposite direction at the edge states, leading to low electron transmission loss.¹⁰⁵ For such 2D materials containing heavy elements, the spin-orbit coupling (SOC) markedly impacts the electronic properties, for instance MXenes with 4d and 5d “M” (Mo, W, Zr, and Hf) will form 2D TIs, and these have broad application prospects in low-power spintronic devices and quantum computing *etc.*¹⁰³ DFT calculations have made great progress in comprehending the electronic properties of MXenes, although the difference between calculated and laboratory properties always exists. Overall, the magic electronic properties of MXenes change from conductor to semiconductor and insulator, and this could give MQDs the potential to be used in many fields.

3.3. Optical properties

The optical properties of MQDs, including light absorption, photoluminescence (PL), electrochemiluminescence (ECL) and so on, are very useful for their applications in biomedical, optoelectronic catalysis, and optoelectronic device fields *etc.*^{1,106} Meanwhile, these properties depend on the synergetic effects of the sizes (*i.e.* quantum confinement), surface chemistry and edge defects, resulting from the different reaction conditions, such as the solvents, filling factors, synthesis temperature,

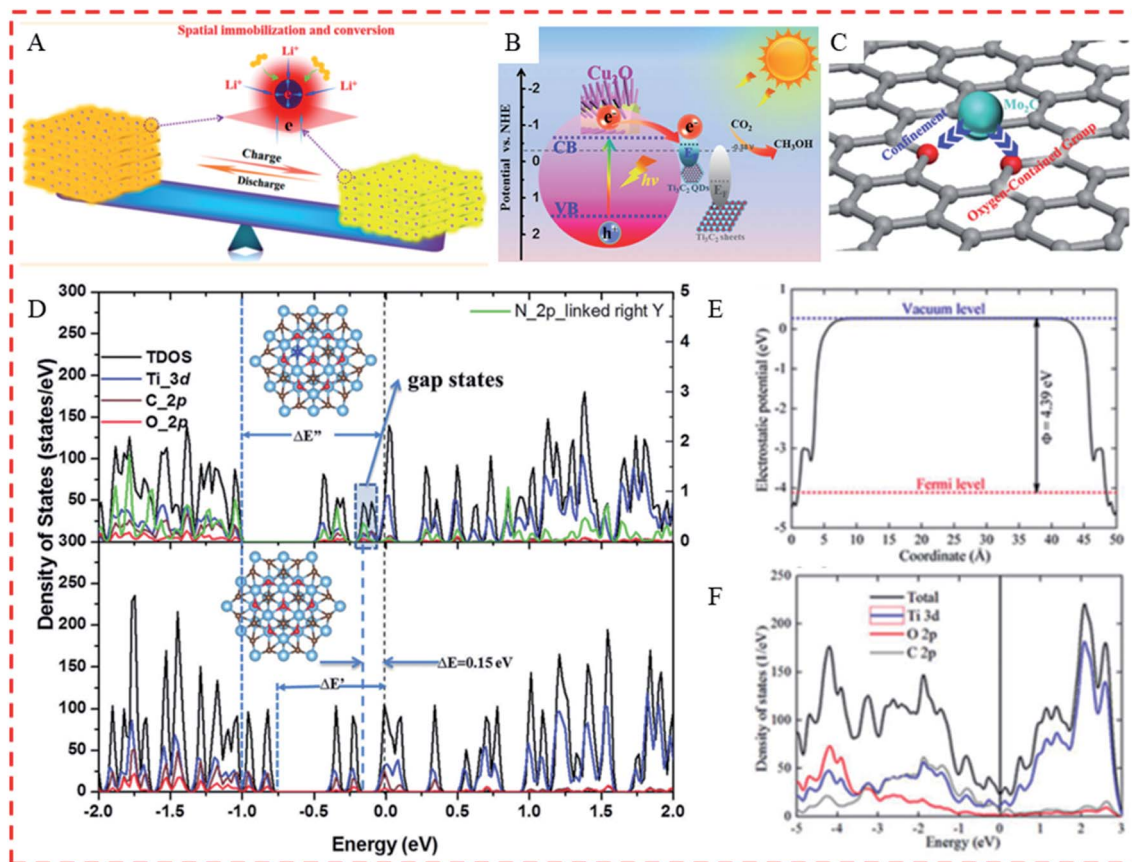


Fig. 7 (A) Schematic illustration for the charge transfer on Ti_3C_2 QDs during the discharge process in a lithium-sulfur battery.³⁹ Copyright 2019 ACS Nano. (B) The electron transfer on Ti_3C_2 QDs in a photocatalytic system.³⁸ Copyright 2019 Advanced Functional Materials. (C) The excellent molecular structure of Mo_2C QDs/C nanosheets for charge transfer in an electrocatalytic system.⁷⁰ Copyright 2018 Advanced Materials. (D) The calculated total and projected DOS of $\text{Ti}_3\text{C}_2\text{O}_2$ QDs (above) and $\text{Ti}_3\text{C}_{2-x}\text{N}_x\text{O}_2$ QDs (below).⁵⁶ Copyright 2018 Journal of Materials Chemistry C. (E and F) The calculated Fermi level and DOS of O-terminated Ti_3C_2 QDs.³⁸ Copyright 2019 Advanced Functional Materials.

duration time and functional modifiers, as well as ambient pH changes.^{1,20,38,56}

Generally, the MQDs have remarkable light absorptivity, ranging from ultraviolet (UV) to near-infrared (NIR) light, due to their adjustable energy band structure by changing their composition and terminated functional groups.^{20,38,107,108} They can convert the absorbed light energy into other energy forms, such as chemical energy, thermal energy, *etc.*, for diversified applications. For example, the Ti_3C_2 QDs could enhance both the efficiency and range of light visible adsorption, thus increasing the photocatalysis activity of the Ti_3C_2 QDs/ Cu_2O nanowire composite (Fig. 8A).³⁸ Moreover, diverse MQDs (Ti_3C_2 QDs, Mo_2C QDs, and V_2C QDs^{20,46,66,69}) exhibit strong absorption in the NIR region and can convert the light energy into heat for photothermal therapy or photothermal assays (Fig. 8B and C).

Compared with the low PL of 2D MXenes, the MQDs achieve strong PL emission. Although the PL mechanism is still controversial, there are two main opinions that are universally accepted, namely size effects and surface defects.^{37,106,109,110} Three main parameters, including PL colour, PL quantum yields (PLQYs) and PL lifetimes (PLLTs), are often investigated

for reflecting the PL behaviors of MQDs.¹ Currently, some studies have reported the PL spectra of MQDs under different excitation wavelengths, showing the excitation-dependent fluorescence emission features in most cases.^{1,41,72} Generally, MQD suspensions are colourless or light yellow or brown, or even black, under daylight due to different reaction synthesis and composition *etc.* (Fig. 3I).⁴¹ However, they emit bright blue or green or red or white or even multicolours under different excitation wavelengths from 355–505 nm, and 365 nm is the most frequently used wavelength (Fig. 8D).⁷² Furthermore, the PL behaviors of MQDs could be tuned by various factors, including synthesis conditions (temperature, solvents or pH *etc.*), MQD size, doping elements and so on.^{37,41,49,51,56,57} For example, Xu *et al.*⁴¹ obtained Ti_3C_2 QDs using different solvents, including DMSO (s-MQDs), ethanol (e-MQDs), and DMF (f-MQDs). Under the 365 nm UV illumination, the obtained QDs system exhibited different PL colors, and these were white (DMSO) and blue (DMF and ethanol), respectively (Fig. 8E). Meanwhile, the PLQYs were measured to be 4.1%, 10.7%, and 6.9%, and the average PLLTs were 4.7 ns, 2.5 ns, and 2.1 ns, for s-MQDs, f-MQDs and e-MQDs, respectively. Xue *et al.*³⁷ reported the PLQYs of the Ti_3C_2

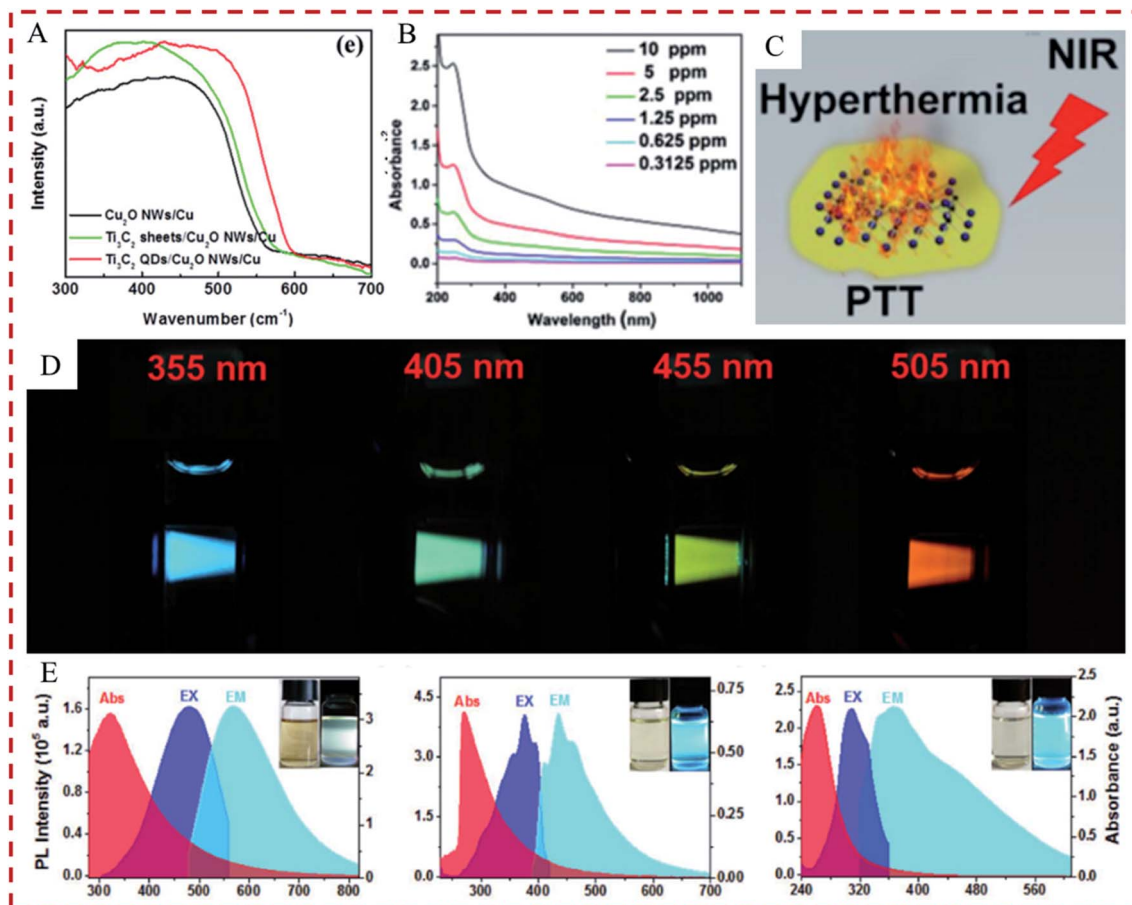


Fig. 8 (A) UV-vis diffuse reflectance spectra of Ti_3C_2 QDs/ Cu_2O nanowires.³⁸ Copyright 2019 Advanced Functional Materials. (B) Absorption spectra of Ti_3C_2 QDs dispersed in water at various concentrations.⁴⁶ Copyright 2017 Nanoscale. (C) Schematic illustration of MXenes QDs converting NIR to heat energy.⁶⁹ Copyright 2018 Materials. (D) PL color of the V_2C QDs under different excitation wavelengths.⁷² Copyright 2019 Advanced Materials. (E) The spectra of UV-vis absorption, maximum excitation (EX) and emission (EM) peaks of the as-prepared Ti_3C_2 QDs. Insets: photographs of the Ti_3C_2 QDs dispersions under 365 nm UV irradiation.⁴¹ Copyright 2018 Advanced Optical Materials.

QDs to be 9.9, 8.7, and 7.9% under the synthesis temperature of 100 °C, 120 °C, and 150 °C, respectively. Meanwhile, the blue PL became heavier with the increase of synthesis temperature under 365 nm light irradiation. Chen *et al.*⁴⁹ found that the PL intensity and lifetime of Ti_3C_2 QDs decreased by increasing the pH value (5–9), which was due to the deprotonation of the surface imperfections in MQDs, and that some luminescent surface imperfections are transformed into non-luminescent surface imperfection locations, thus acting as non-radiative passages for capturing carriers, resulting in the reduction of the emission intensity of MQDs (Fig. 9A and B). Furthermore, heteroatom doping also significantly changed the PL behavior.^{3,57} For example, the doped Ti_3C_2 QDs showed different fluorescence under 365 nm UV irradiation by doping different elements, and they corresponded to blue, yellow and orange fluorescence for S-MQDs (7.74 ns, 28.12%), N-MQDs (5.81 ns, 8.33%) and SN-MQDs (4.67 ns, 7.78%) (Fig. 9C–E), respectively.³ The change in their PL behaviors can be attributed to the fact that the different synthesis conditions will produce MQDs with different sizes, morphologies, defect degrees, and surface/edge states.^{37,109,110}

In addition to PL properties, ECL is also considered to be an important optical property that can be used to evaluate the capabilities of MQDs and expand their applications. ECL is a method of converting electrical energy into an easily detectable fluorescence signal. By combining the advantages of electrochemistry and chemiluminescence, ECL can be considered as a more effective analytical tool by significantly eliminating background interference. The merits of ECL, such as high sensitivity, a broad detection range and easy extension endow it with promising applications in biosensing, cell-imaging, *etc.*^{54,111} However, the ECL of the MQDs has had limited studying until now. Qin *et al.*⁵⁴ first reported the ECL properties of MQDs (Ti_3C_2 QDs) in detail *via* an annihilation operation and a co-reactant enhancement process. The results showed that the MQDs could entice a strong ECL signal on the time scale from 0 to 1050 s (Fig. 9F and G). The probable ECL generation pathway could be as follows: first, both negatively charged MQDs ($\text{MQDs}^{\cdot-}$) and positively charged MQDs ($\text{MQDs}^{\cdot+}$) are formed by reducing or oxidizing MQDs (eqn (1) and (2)). Then, the excited state of MQDs (MQDs^*) was produced after the diffusing and colliding of $\text{MQDs}^{\cdot-}$ and $\text{MQDs}^{\cdot+}$ (eqn (3)). Finally, unstable MQDs^* were readily converted into the ground

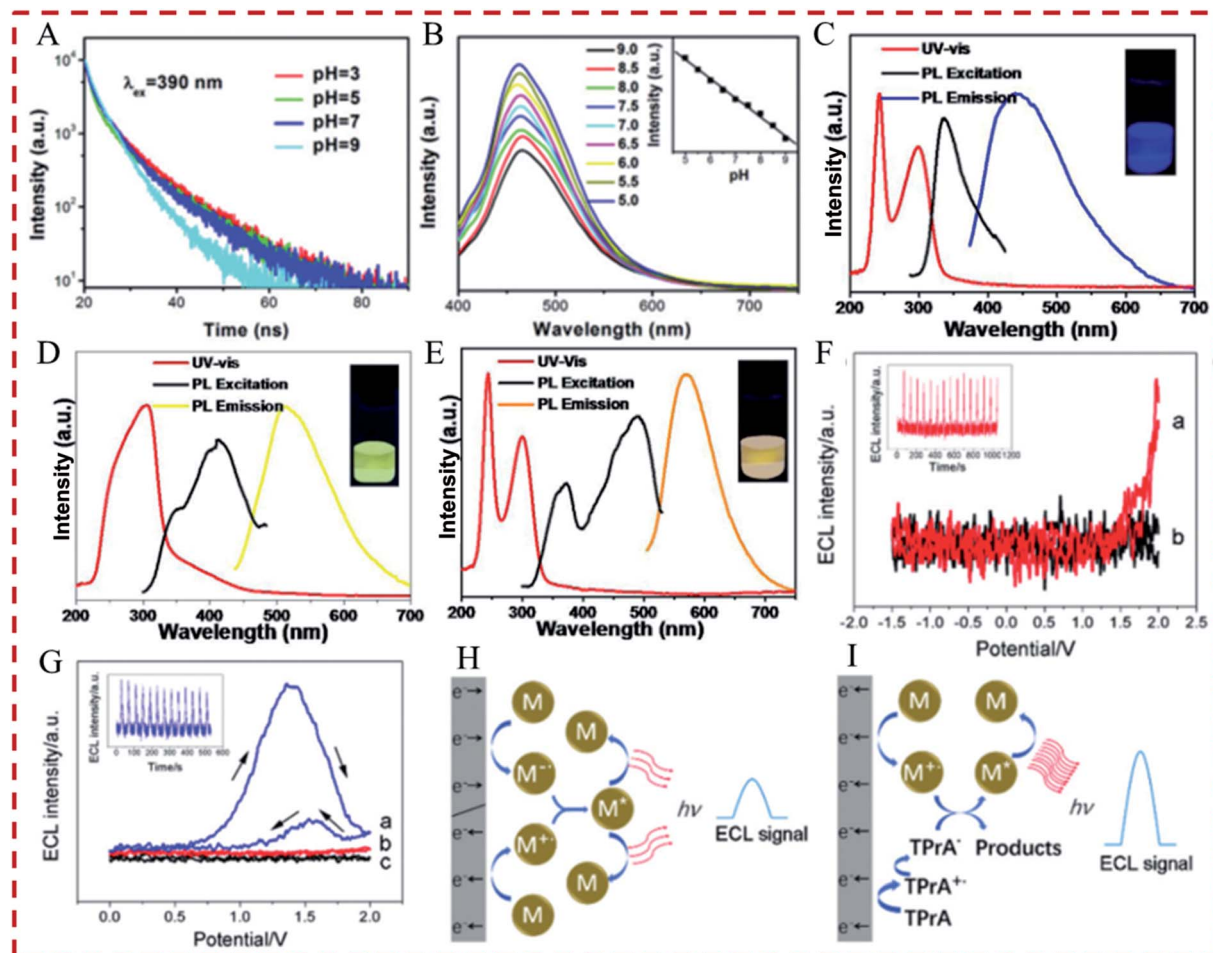
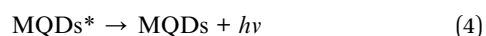
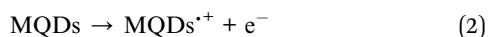
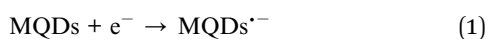


Fig. 9 (A) Photoluminescence decay of Ti_3C_2 QDs aqueous solution at 460 nm under 390 nm excitation at 25 °C with different pH values.⁴⁹ Copyright 2018 Nanoscale. (B) Emission spectra of Ti_3C_2 QDs in aqueous solution with different pH values ($\lambda_{\text{ex}} = 350$ nm).⁴⁹ Copyright 2018 Nanoscale. (C–E) UV-vis absorption spectra and PL spectra (excitation and emission scans) under 360 nm UV irradiation of S- Ti_3C_2 QDs, N- Ti_3C_2 QDs and SN- Ti_3C_2 QDs. Inset (top-right): photographs of Ti_3C_2 QDs under 365 nm UV irradiation.³ Copyright 2019 Applied Materials Today. (F) Annihilation ECL response.⁵⁴ Copyright 2018 Nanoscale. (G) Anode ECL response.⁵⁴ Copyright 2018 Nanoscale. (H) Schematic presentation of an annihilation ECL pathway.⁵⁴ Copyright 2018 Nanoscale. (I) Schematic mechanism of the TPrA enhanced ECL pathway.⁵⁴ Copyright 2018 Nanoscale.

state of MQDs by emitting photons, thus generating an ECL signal (Fig. 9H) (eqn (4)).



In addition, the co-reactant enhancement processes of Ti_3C_2 QDs were studied by employing some kind of common cathode or anode co-reactants: TPrA, $\text{Na}_2\text{C}_2\text{O}_4$, H_2O_2 , and $\text{K}_2\text{S}_2\text{O}_8$, and the results indicated that TPrA exhibited a better promoting effect (~29-fold) in the anode ECL process (Fig. 9I). Furthermore, the stability experiments have shown that MQDs are a robust ECL luminophore, and this verified that the MQDs have potential in ECL sensing. Afterwards, Xu *et al.*⁴¹ also

reported the ECL performance of $\text{Ti}_3\text{C}_2\text{T}_x$ QDs in the existence of a co-reactant ($\text{K}_2\text{S}_2\text{O}_8$, L-cysteine, citric acid, H_2O_2 , or glutathione), and the results indicated that the ECL activity clearly improved by employing $\text{K}_2\text{S}_2\text{O}_8$ as a co-reactant.

Apart from the commonly studied PL and electrochemiluminescence properties of MQDs, their up-conversion PL optical properties and transparent optical properties should also be given more attention.^{1,112} Up-conversion PL is a phenomenon whereby the PL emission wavelength is shorter than the used excitation wavelength, in other words the photon energy of emission is higher than that of excitation. Therefore, when using MQDs in photoelectric materials, they will show increased efficiency in the use of light energy.^{113,114} The transparent optical properties of the materials, combined with their electrical conductivity have attracted considerable attention for their potential application in transparent conducting films, which could be applied in various futuristic photoelectric devices, including touch panels, photovoltaics, smart windows,

liquid crystal displays, transparent sensors, transparent heaters, supercapacitors, and so on. To date, 2D MXene materials have been widely studied in transparent conducting films,^{112,115–118} however there have been no related studies of MQDs. The excellent optical properties of MQDs enable them to have broad application prospects in many fields. Nevertheless, up to now, most research has only concentrated on the PL properties, and more attention and effort should be paid to other optical properties, as this is of great significance to their development and application.

3.4. Magnetic properties

Magnetic properties are important physical properties that can be used in a variety of biomedical fields. The MAX phases, in which the “M” is Cr and/or Mn, almost all performed magnetism, *e.g.* Cr₂AlC, Cr₂GeC, Cr₂GaC, Cr₂AlN, C₂GaN, Mn₂AlC, Mn₂GaC, Cr₂TiAlC₂, and (Cr_{2/3}Sc_{1/3})₂AlC.⁴² However, so far, the magnetic properties of MXenes have rarely been demonstrated by experimental research, only the DFT calculations have forecast that several bare and terminated MXenes exhibit magnetism. According to the theoretical studies, the non-spin

polarized DOS at the E_F performed high value should signify magnetic instability, and the M₂X and M₃X₂ families are deemed magnetic. In view of the magnetism of “M” atoms, they could be divided into ferromagnetic (FM) and antiferromagnetic (AFM, A-type, C-type and G-type) according to the TM spin in single unit structures of MXenes, as shown in Fig. 10A.⁹⁹ Compared to un-terminated MXenes, the magnetic performance of MXenes relies on the composition of M and X, and on the terminations. In a recent study, five different nitride MXenes (Mn₂NF₂, Mn₂NO₂, Mn₂N(OH)₂, Ti₂NO₂, and Cr₂NO₂), as well as Mn₂C and F/OH-terminated Mn₂C, have been predicted to exhibit a FM ground-state, however O-terminated Mn₂C and most of the surface-terminated MXenes showed an AFM ground-state. The different magnetic ground states for carbide and nitride MXenes results from the additional electron supplement by nitrogen. Furthermore, their crystal tension has also marked influence on the magnetic properties, and element-doping and vacancy-introducing are two frequently used methods for regulating their magnetic properties.⁴³ Recently, Cao *et al.*²⁰ revealed the good magnetic resonance capability of the V₂C QDs-based nanomaterial and this could be applied for

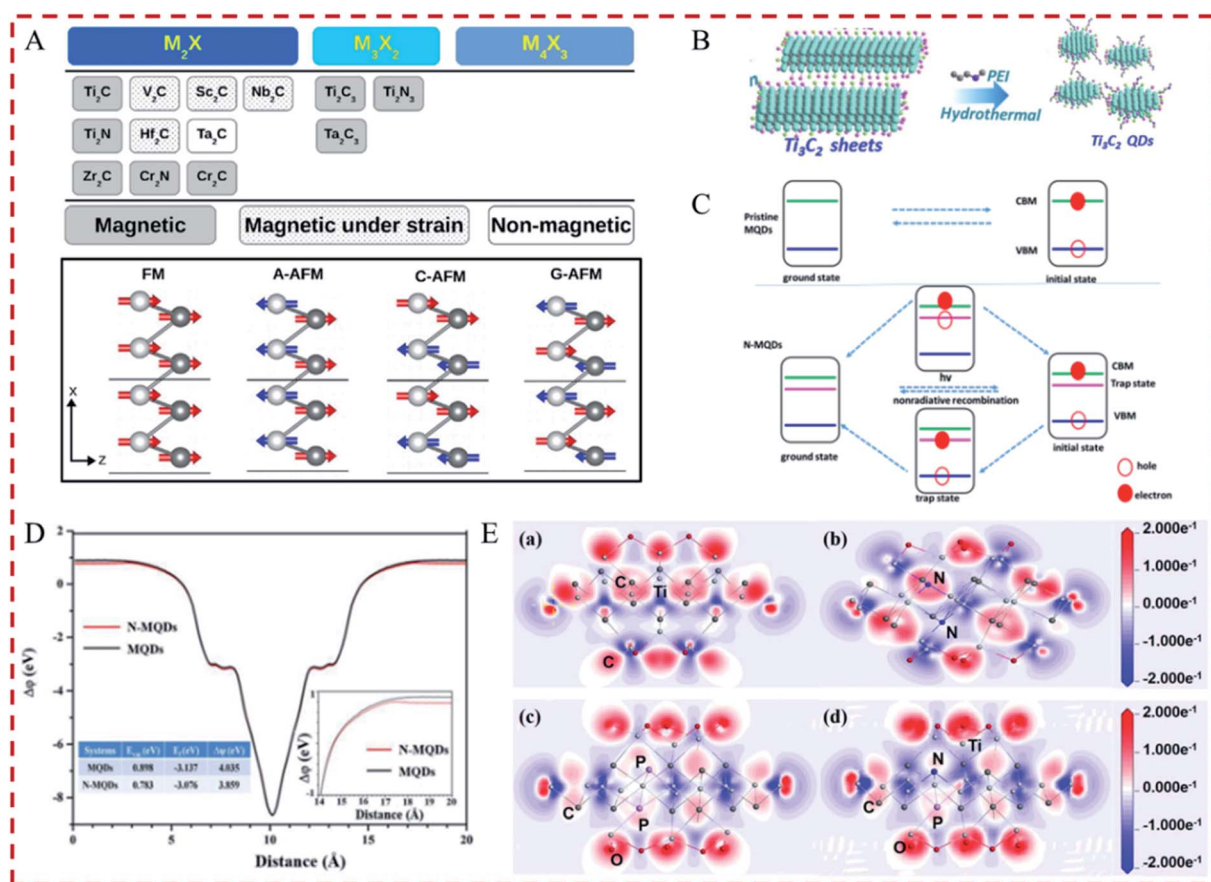


Fig. 10 (A) The various unpassivated magnetic MXenes belonging to M₂X, M₃X₂, M₄X₃ families, and the various possible magnetic states in M₂X.⁹⁹ Copyright 2019 Comprehensive Nanoscience and Nanotechnology. (B) Schematic illustration for the surface modification of Ti₃C₂ QDs by PEI.⁹⁸ Copyright 2019 Advanced Functional Materials. (C) Diagram of the energy levels and charge-transfer processes inside the Ti₃C₂ QDs and N-Ti₃C₂ QDs.⁵⁶ Copyright 2018 Journal of Materials Chemistry C. (D) Working function of pristine Ti₃C₂ QDs and N-Ti₃C₂ QDs.⁵⁶ Copyright 2018 Journal of Materials Chemistry C. (E) The charge density difference of the pure MXene QDs and heteroatom functionalized Ti₃C₂ QDs: (a) pure Ti₃C₂ QDs, (b) N-Ti₃C₂ QDs, (c) P-Ti₃C₂ QDs and (d) N, P-Ti₃C₂ QDs.⁵⁷ Copyright 2019 Nanoscale.

multi-model imaging in clinical applications. Although there is little research on magnetic properties of MQDs, these theoretical studies will provide guidance for investigating the MQDs.

3.5. Functionalizations

Due to some inevitable disadvantages of MQDs, such as aggregation, oxidation, functionalization is often performed in order to improve their practical applications, and the common functionalization methods include surface modification, heteroatom doping and constructing composites.^{27,38,56,58} It is clear from the above discussion that the outer surfaces of MQDs are currently passivated with $-O$, $-F$ or $-OH$ functional groups caused in the synthesis process, and this is the most direct surface modification method and thus significantly impacts the properties and stability of MQDs.¹¹⁹ Apart from these functional groups, other special functional groups, like the $-NH$ group, were also frequently introduced to modify the surface of MQDs by adding ammonia in the synthesis process.^{37,51,72} Furthermore, modifying the surface of MQDs by an organic compound can be another effective method. For instance, Zeng *et al.*^{38,49} reported Ti_3C_2 QDs grafted with positively charged polyethylenimine (Fig. 10B). Cao *et al.*²⁰ synthesized TAT peptide and poly(ethylene glycol) modified V_2C QDs. The surface modification will significantly augment the performance of MQDs, such as the dispersibility, biocompatibility, targeting capacity, stability, and so on.^{27,120–122} In addition to surface modification, heteroatom doping can be another effective method to tune the properties of MQDs. It is well known that heteroatom doping is an efficient and simple method to endow or improve the electromagnetic, physicochemical, optical, and structural properties of materials.^{123,124} To date, there have been several studies on the use of non-metallic element (N, P, and S) doped/co-doped Ti_3C_2 QDs. The results indicated that heteroatom doping will distinctly optimize the properties of MQDs (Ti_3C_2 QDs) and, compared to single element doping, co-doping might enable better results. For example, Xu *et al.*⁵⁶ reported N- Ti_3C_2 QDs, and the results indicated that the N element doping clearly increased the light absorption. Moreover, the element doping will significantly improve the electronic properties of Ti_3C_2 QDs, resulting in the E_g widening (Fig. 7D). Based on the mechanism of the carrier life (Fig. 10C), it can be seen that N- Ti_3C_2 QDs are beneficial to reducing the charge and energy loss, thus accelerating electron transfer, increasing the lifetime of the carrier and improving PLQYs (18.7%). Furthermore, the N-MQDs possess lower WF, suggesting that the electron transfer is easier (Fig. 10D). Guan *et al.*⁵⁷ reported N-doped, P-doped and N, P-co-doped Ti_3C_2 QDs. The DFT calculations indicated that the heteroatom doping could cause charge transfer, thus improving the optical properties of Ti_3C_2 QDs (Fig. 10F). The improved optical and electronic properties of MQDs will enable them to be applied effectively in biomedical and optoelectronic fields. In addition, combining MQDs with other materials to form a composite is also a common method for improving their performance and expanding their application. Up to now, there have been

multitudinous kinds of materials, such as carbons, semiconductors, biomaterials, and inorganic nonmetallic materials that have been successfully hybridized with MQDs to design hybrid nanocomposites *via* hydrothermal, ball-milling and other methods, such as Ti_3C_2 QDs/ TiO_2 , Ti_3C_2 QDs/ Cu_2O nanowires, Ti_3C_2 QDs/liposomes, Ti_3C_2 QDs/ $Ti_3C_2T_x$ nanosheets, Mo_2C QDs/carbon, Ti_3C_2 QDs/P (or C, or S, or Si) *etc.*^{20,38,39,48,65,66,70,71} The incorporation of MQDs into other materials can not only improve their dispersion, stability and recycling *etc.*, but it can also optimize the performance of the combined material, and these composites exhibit great promise in sensing, biomedical, catalysis and energy storage fields *etc.* (more detailed discussion can be found in Section 4). Although there is still limited research on MQDs, the functionalization of MQDs is key to implementing their practical application, and so more effective functionalization methods also need to be further studied.

4. Applications of MQDs

4.1. Sensing

4.1.1. Metal ion detection. Over the past few decades, a large number of metal ions, such as Fe^{3+} , Cr^{2+} , Pb^{2+} , Cu^{2+} , Zn^{2+} , *etc.*, have been released into water with the development of industries, and this will destroy the water ecosystem and threaten the safety of humans.^{73,125–130} Thus, the development of an effective metal ion detecting technique is the prerequisite for the prevention and control of heavy metal pollution.^{131–135} Recently, the fluorescence-based QD biological sensing for metal ion detection has aroused great interest due to its high sensitivity, low detection limit, good selectivity, wide detection range, fast response, good anti-jamming ability and ease of operation, *etc.*^{136–140} To date, there have also been some studies on metal ion (especially for Fe^{3+}) detection using MQDs, based on the PL quenching mechanism.^{41,55–57,63,68,73} For instance, Xu *et al.*⁵⁶ reported that the N-doped $Ti_3C_2T_x$ QDs performed with fine sensitivity and selectivity for Fe^{3+} detection, and the results showed that the detectable concentration was in the range of 2–5000 μM , the limit of detection (LOD) was 2.0 μM , and the detection time was only 0.5 min. Meanwhile, the good selectivity of N-MQDs was studied in the presence of other different metal ions (Na^+ , Mg^{2+} , Cu^{2+} , K^+ , Mn^{2+} , Zn^{2+} , Ca^{2+} , Al^{3+} , Ce^{3+} , Cu^+ and Ni^{2+}) (Fig. 11A and B). Except for Fe^{3+} , the Ti_3C_2 QDs also showed the efficient detection of Zn^{2+} ,³⁷ Cu^{2+} ,⁵⁷ Ag^+ and Mn^{2+} .⁶³ The most acceptable PL quenching mechanism was the mechanism involving the oxygenous groups, *e.g.* hydroxyl, carboxyl and carbonyl, on the surface and edge of the MQDs, where the metal ion acts as a coordinating center to bridge well-dispersed MQD individuals together *via* high-affinity interactions between the metal ion and the oxygenous functional groups. Subsequently, this affinity interaction results in aggregation-induced PL quenching of the MQDs.^{141,142}

4.1.2. Protein detection. Compared to metal ion detection, the direct detection of biological substances, such as an enzyme, an antigen *etc.*, by an MQDs probe should be more efficient for biological sensing applications.^{52,53,143–145} To date, there are several studies on Ti_3C_2 QDs for detecting biological

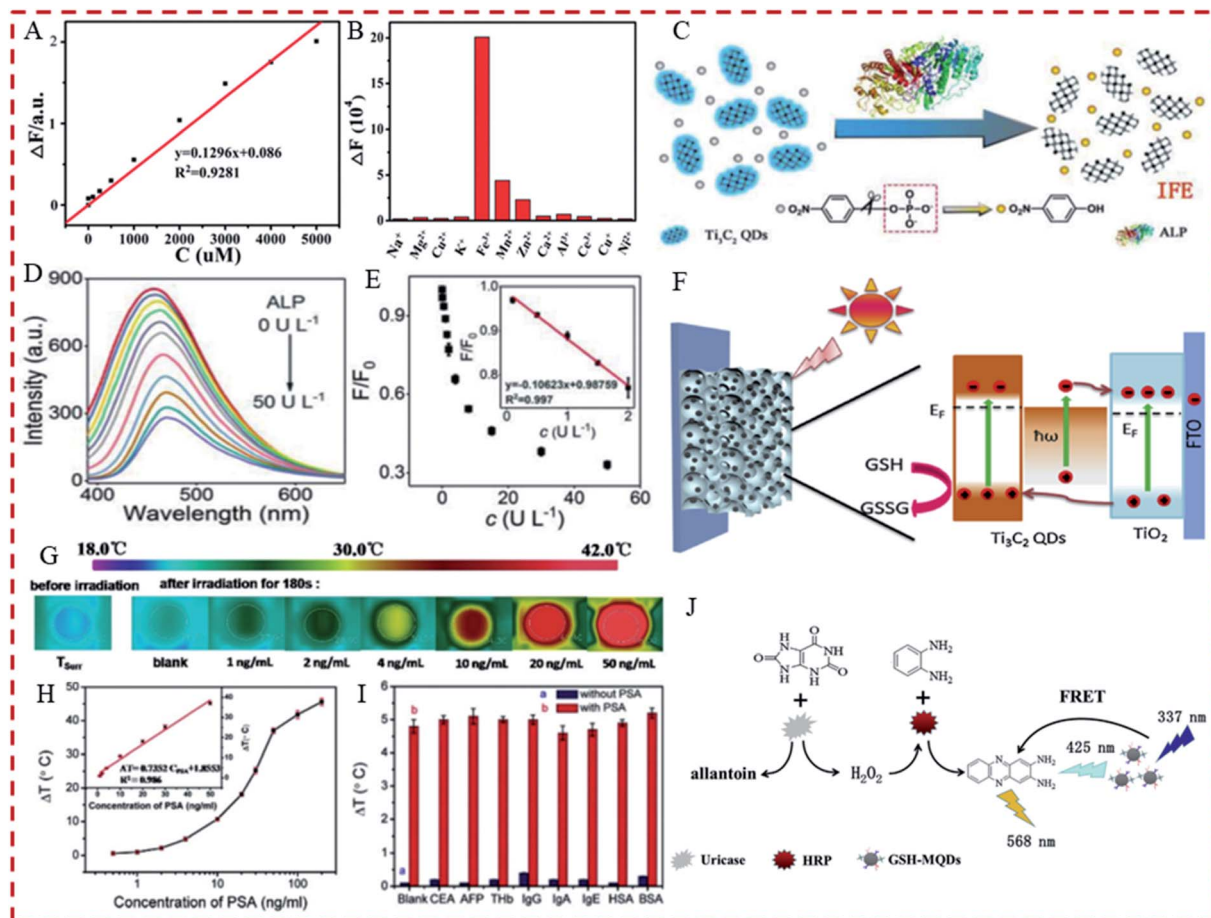


Fig. 11 (A) ΔF calibration curve of the N- Ti_3C_2 QD solution versus the concentration of Fe^{3+} .⁵⁶ Copyright 2018 Journal of Materials Chemistry C. (B) The change in fluorescence intensity at 447 nm for N- Ti_3C_2 QDs in the presence of various metal ions.⁵⁶ Copyright 2018 Journal of Materials Chemistry C. (C) Schematic illustration of the Ti_3C_2 QD-based fluorescence assay for ALP activity.⁵¹ Copyright 2019 Nanoscale. (D) Fluorescence emission spectrum of Ti_3C_2 QDs in the presence of different concentrations of ALP with 200 μM *p*-NPP.⁵¹ Copyright 2019 Nanoscale. (E) Plots of fluorescence response (F/F_0) versus ALP concentration (inset: the linear relationship from 0.1 to 2.0 U L^{-1}).⁵¹ Copyright 2019 Nanoscale. (F) PEC mechanism for the Ti_3C_2 QDs/ TiO_2 electrode with the illumination of standard solar lights.⁶⁵ Copyright 2019 Sensors and Actuators B: Chemical. (G) Photographs of the thermal immunoassay relative to PSA standards from 0 to 50 ng mL^{-1} .⁶⁶ Copyright 2019 Nanoscale. (H) The temperature variation with different concentrations of PSA (inset: the linear curve).⁶⁶ Copyright 2019 Nanoscale. (I) The selectivity of the photothermal immunoassay towards the target PSA in the absence and presence of interfering agents.⁶⁶ Copyright 2019 Nanoscale. (J) Schematic diagram of uric acid based on GSH- Ti_3C_2 QDs based on the enzymatic reaction catalyzed by uricase and HRP.⁵⁹ Copyright 2020 Analytica Chimica Acta.

substances. For instance, Guo *et al.*⁵¹ used Ti_3C_2 QDs for an alkaline phosphatase (ALP) assay according to the inner filter effect (IFE). The results indicated that the fluorescence intensity of Ti_3C_2 QDs decreased by a few degrees with an increase in ALP concentration from 0 to 50 U L^{-1} , and a good linearity between the quenching efficiency and ALP concentration, ranging from 0.1 to 2.0 U L^{-1} , was obtained, and the LOD was 0.02 U L^{-1} . The detection mechanism is due to the significant overlap between the absorption spectrum of *p*-nitrophenol and the excitation and emission spectra of Ti_3C_2 QDs (*p*-nitrophenol is produced from the ALP-catalyzed dephosphorylation of the substrate), thus effectively quenching the fluorescence of Ti_3C_2 QDs by IFE (Fig. 11C–E). Chen *et al.*⁶⁵ also reported the Ti_3C_2 QD-based heterojunction (Ti_3C_2 QDs/ TiO_2) electrode for superior photoelectrochemical (PEC) biosensing of glutathione. The electrode showed high stability, sensitivity, and selectivity for the detection of

glutathione in both buffered solution (0.1–1000 μM , LOD was 0.9 nM) and cell extracts (1–200 μM , LOD was 0.55 μM) (Fig. 11F). Furthermore, Cai *et al.*⁶⁶ designed an NIR photo-thermal immunoassay for high sensitivity and selectivity of prostate-specific antigen (PSA) detection using Ti_3C_2 QD-encapsulated liposomes. The results showed that the Ti_3C_2 QDs converted the light energy into heat under NIR-laser irradiation, and a shift in temperature, corresponding with the analyte concentration, was acquired on a handheld thermometer. Under optimal conditions, the Ti_3C_2 QD-based photothermal immunoassay exhibited a dynamic linear range from 1.0–50 ng mL^{-1} for PSA detection, and the LOD reached 0.4 ng mL^{-1} (Fig. 11G–I). The above studies indicated that the prepared MQDs could be perfect bioprobes for the efficient detection of cell biological characteristics, and can be used for cell health monitoring and biosensors.

4.1.3. Detection of other molecules. In addition, the MQDs have been studied for the detection of other substances. For instance, Xu *et al.*⁵⁶ has prepared nitrogen-doped Ti_3C_2 QDs (N-MQDs), and the possibility of detecting H_2O_2 with the aid of Fe^{2+} was investigated. The results indicated that no observable fluorescence intensity change was noted in the presence of 50 mM H_2O_2 solution, suggesting that the PL of N-MQDs could not be quenched by H_2O_2 alone. However, when H_2O_2 and Fe^{2+} simultaneously exist, the PL intensity of N-MQDs is reduced significantly (reaching 69.78%), indicating that the N-MQDs could be used as a probe for H_2O_2 detection. Chen *et al.*⁴⁹ developed an intracellular pH sensor based on poly-ethylenimine functionalized Ti_3C_2 QDs. The synthetic Ti_3C_2 QDs exhibited favorable pH dependent luminescence behavior, thus integrating the highly pH sensitive Ti_3C_2 QDs with the pH insensitive $[\text{Ru}(\text{dpp})_3]\text{Cl}_2$, resulting in a pH sensor to quantitatively detect the intracellular pH values being developed. Liu *et al.*⁵⁹ has reported glutathione functionalized Ti_3C_2 QDs (GSH- Ti_3C_2) for the detection of uric acid, based on the oxidation of uric acid by uricase to allantoin and hydrogen peroxide, and then *o*-phenylenediamine (OPD) was oxidized to the yellow-colored 2,3-diaminophenazine (oxOPD) in the presence of horseradish peroxidase (HRP) and hydrogen peroxide (Fig. 11J). The results indicated that the fluorescence emission of GSH- Ti_3C_2 QDs centered at 430 nm overlaps with the UV absorption of oxOPD at 425 nm to a large extent, and this facilitates fluorescence resonance energy transfer (FRET) between GSH- Ti_3C_2 QDs and oxOPD. With the increase in uric acid concentration, the emission at 430 nm of the GSH- Ti_3C_2 QDs is progressively quenched and the emission at 568 nm of oxOPD gradually increased.

4.2. Biomedical

4.2.1. Bioimaging. Bioimaging is an effective study technique in the field of modern biology and medicine that can provide clear and intuitive biological information for researchers by a quick and easy method.^{136,146,147} To date, many semiconductor QDs have been studied in this field, however they usually contain toxic heavy metals that limit their practical application.¹⁴⁸ Compared to semiconductor QDs, the non-toxic or low-toxic nature of MQDs generally result in better biocompatibility in bioimaging, and it is therefore expected to be a remarkable bioimaging material.¹⁴⁹ To date, several studies have demonstrated the excellent bioimaging capability of MQDs based on their PL properties.^{37,46,47,49,57,69,73}

For instance, Xue *et al.*³⁷ first reported the PL Ti_3C_2 MXene QDs for multicolor cellular imaging. The as-prepared Ti_3C_2 QDs exhibited excitation-dependent PL spectra with PLQYs of about 10%, due to effective quantum confinement. The cytotoxicity experiments showed that the Ti_3C_2 QDs possess low cytotoxicity for RAW264.7 cells, and they were readily ingested *via* endocytosis. The confocal images showed bright blue, green, and red colors at the excitation of 405, 488 and 543 nm, respectively. Furthermore, according to the confocal luminescence images, it can be observed that the QDs primarily exist in the cell membrane and in the cytoplasm, and very weak luminescence

points were shown in the nucleus region (Fig. 12A), suggesting that the QDs can readily diffuse into the cell without entering the nucleus and resulting in genetic damage. Cao *et al.*²⁰ employed a V_2C QD-based nanocomposite to acquire bioimaging of MCF-7 and NHDF cells. The results showed that the nanocomposite enabled entering into both MCF-7 and NHDF cells by the endocytic uptake pathway (Fig. 12B and C). These studies showed that MQDs exhibit great application prospects in biological and medical fields in a safe and efficient way.

4.2.2. Photothermal therapy. In recent years, the photothermal therapy (PTT) employing NIR illumination for tumor hyperthermia ablation has been widely studied and has received great enthusiasm. As the local heat can be well controlled in temporal and spatial lobes, PTT exhibits fewer side effects than traditional tumor therapeutic methods.²⁰ Recently, diverse 2D materials, including MXenes, have been frequently explored as photothermal agents (PTAs) for *in vitro* and *in vivo* PTT applications. However, the low photothermal conversion efficiency (PTCE) and the large size in dimension of 2D materials still limit their practical use in PTT.^{150–152} Hence, there is a huge demand for developing ultra-small PTAs with high PTCE and without toxicity concerns, in order to acquire a high-efficiency photothermal tumor treatment.⁴⁶ Attractively, the emerging MQDs could be satisfactory PTAs, due to their excellent NIR adsorption and biocompatibility properties.^{20,46,69} For example, Cao *et al.*²⁰ developed V_2C QD-based (V_2C QDs-TAT peptides/exosomes) PTAs for eliminating tumors by PTT. The ultra-small V_2C QDs exhibited a strong photothermal effect in the NIR-II region, and the PTCE was up to 45.05%. The V_2C QD-based PTAs had favorable biocompatibility and circulation ability, and they could easily target the cancer cells and penetrate into the nucleus. Under the illumination of the NIR-II region, the PTA-mediated nucleus temperature increased, causing genetic material to be destroyed and protein denaturation, thus resulting in the death of cancer cells both *in vitro* and *in vivo* (Fig. 12D and E). Furthermore, the Ti_3C_2 QDs⁴⁶ and Mo_2C QDs⁶⁹ also exhibited the high-efficiency PTT effect on tumors both *in vitro* and *in vivo* under NIR illumination. These studies suggest that the MQDs will initiate a new era in the PTT of tumors.

4.2.3. Immunomodulation. Combining the fields of biomaterials, regenerative medicine and immunology will help to develop new therapies for treating inflammatory and degenerative diseases. The next-generation of intelligent biomaterials are playing an increasingly important part in advancing treatment options for different diseases.^{40,145,147,153} Recently, the development of MQDs with distinguished structural and biomedical properties endows them with great application potential in this field due to their excellent structural and biomedical properties. Rafieerad *et al.*⁴⁰ first reported that the Ti_3C_2 QDs could be used for immunomodulation with improving material-based tissue repair after injury. In particular, the Ti_3C_2 QDs have intrinsic immunomodulation characteristics and can selectively decrease the activation of human $\text{CD4}^+\text{IFN-}\gamma^+$ T-lymphocytes (control: $87.1 \pm 2.0\%$, Ti_3C_2 QDs: $68.3 \pm 5.4\%$), while facilitating the expansion of immunosuppressive $\text{CD4}^+\text{CD25}^+\text{FoxP3}^+$ regulatory T-cells (control: $5.5 \pm$

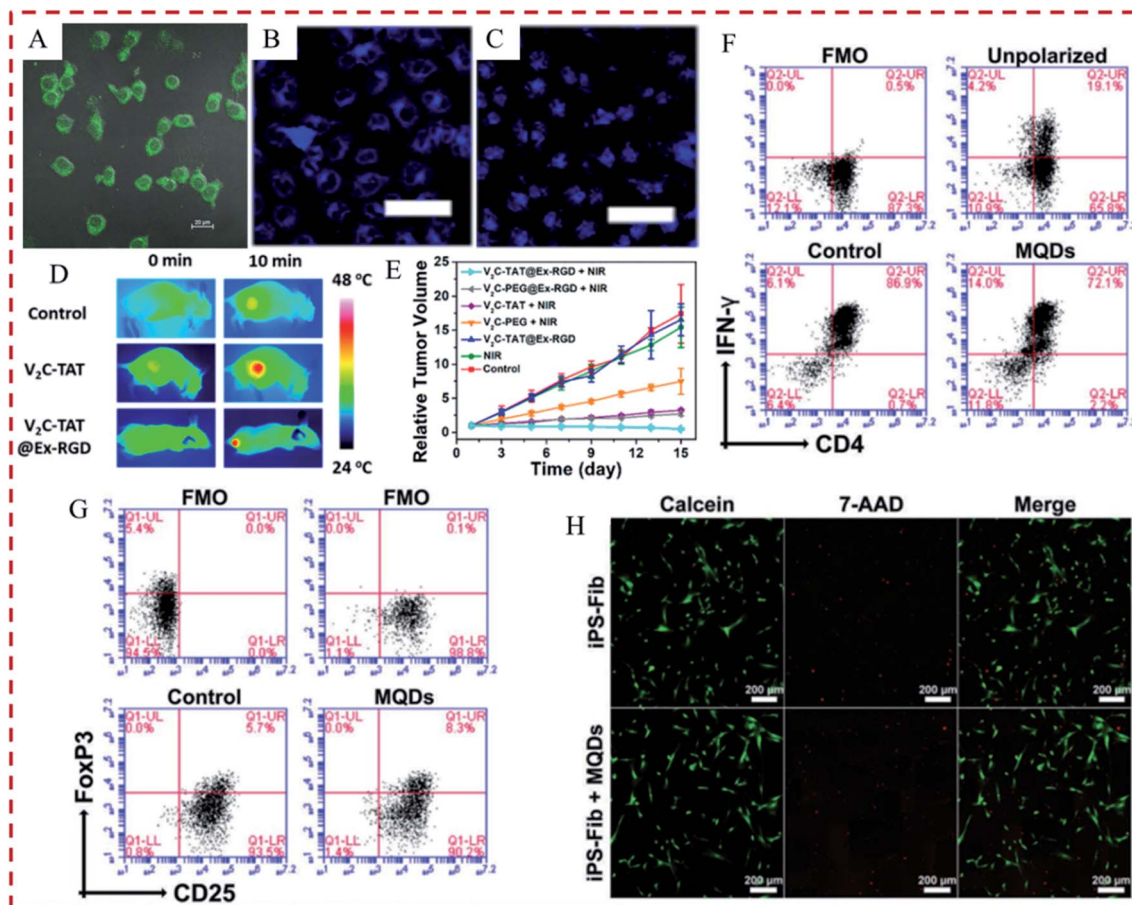


Fig. 12 (A) Bioimaging image of RAW264.7 cells after up-taking Ti_3C_2 QDs.³⁷ Copyright 2017 Advanced Materials. (B and C) Bioimaging images of MCF-7 and NHDF cells after up-taking the V_2C QD-based nanocomposite.²⁰ Copyright 2019 ACS Nano. (D) IR thermal images at the tumor sites of MCF-7 tumor-bearing mice after NIR laser irradiation.²⁰ Copyright 2019 ACS Nano. (E) Relative tumor growth curves of the MCF-7 tumor-bearing mice in a different V_2C QD-based nanocomposite.²⁰ Copyright 2019 ACS Nano. (F) Flow cytometry phenotyping was performed on stimulated human $\text{CD}4^+\text{IFN-}\gamma^+$ T-lymphocytes after 7 days of culture.⁴⁰ Copyright 2019 Advanced Healthcare Materials. (G) Identification of $\text{CD}4^+\text{CD}25^+\text{FoxP}3^+$ regulatory T-cells.⁴⁰ Copyright 2019 Advanced Healthcare Materials. (H) Ti_3C_2 QDs were subsequently cocultured with human iPSC-derived fibroblasts for 24 h and subsequently stained for live and dead cells.⁴⁰ Copyright 2019 Advanced Healthcare Materials.

0.7%, Ti_3C_2 QDs: $8.5 \pm 0.8\%$) in a stimulated lymphocyte population (Fig. 12F and G). Meanwhile, Ti_3C_2 QDs are biocompatible with bone marrow-derived mesenchymal stem cells and induced pluripotent stem cell-derived fibroblasts (Fig. 12H). Furthermore, Ti_3C_2 QDs were integrated into a chitosan-based hydrogel to construct a 3D platform with improved physicochemical properties for stem cell delivery and tissue repair. This composite hydrogel demonstrated increased conductivity whilst maintaining injectability and thermosensitivity. Although the related studies are still limited, these exciting results should promote further research on the use of MQDs in clinically translatable applications.

4.3. Catalysis

Recently, great advances have been made in the development of QD materials, including graphene QDs, carbon QDs, $\text{g-C}_3\text{N}_4$ QDs, BP QDs and TMDs QDs *etc.*, as high-efficiency catalysts/cocatalysts in catalysis systems.^{154–156} Due to the emergence of MQDs, they are considered to be promising catalysts/co-

catalysts, and the main reasons may be that: (a) they possess the native properties of their 2D MXene counterparts, including the functionalization by surface groups ($-\text{OH}$, $-\text{O}$ and $-\text{F}$), the wonderful electroconductibility, the adjustable band structure, and so on; (b) they possess low toxicity, unique photochemical robustness, tunable optical properties and excellent catalytic abilities.^{14,38,58,70}

4.3.1. Electrocatalysis. Electrocatalysis is an efficient advanced oxidation process (AOP), which was unremittably studied in energy and environmental applications, *e.g.* in the hydrogen evolution reaction (HER), the oxygen reduction reaction (ORR), the methanol oxidation reaction (MOR), in nitrogen fixation, and so on.^{58,70,157,158} Recent progresses in DFT calculations have verified that the MXene materials have a large DOS around E_F , and this endows them with promising electrocatalytic activity. Although many studies have been concentrated on the application of 2D MXenes in electrocatalysis up to now, recently research on MQDs in electrocatalysis has just begun to emerge.

The electrocatalytic ORR and MOR are essential to renewable-energy technology,¹⁵⁷ so the excellent properties of

MQDs would enable them to play an important role in the electrocatalytic system. Yang *et al.*⁵⁸ reported a unique composite of multiwalled carbon nanotubes (MWCNTs) embellished by MoS₂ QDs and Ti₃C₂T_x QDs (MoS₂ QDs@Ti₃-C₂T_x QDs@MWCNTs), and employed them for ORR and MOR in alkaline solution by electrocatalysis. The results showed that the excellent electrochemical performance and size dependent quantum confinement of the Ti₃C₂T_x QDs could effectively accelerate electron transfer and provide more active sites, thus endowing the MoS₂ QDs@Ti₃C₂T_x QDs@MWCNTs composite with outstanding electrocatalytic performance and stability for ORR and MOR. Furthermore, nitrogen fixation by electrocatalysis is also deemed as a promising method to acquire high NH₃ production, which plays an important role in human development and industrial progress. However, due to the chemical inertness of nitrogen, it is necessary to explore high-efficiency catalysts for promoting the reduction of nitrogen.^{70,159,160} Cheng *et al.*⁷⁰ found that Mo₂C QDs anchored on ultrathin carbon nanosheets (Mo₂C/C) could act as an efficient electrocatalyst for the nitrogen reduction reaction (NRR). The prepared Mo₂C/C composite exhibited remarkable electrocatalytic activity for NRR with the NH₃ yield rate up to 11.3 μg h⁻¹ mg⁻¹, and the faradaic efficiency was 7.8% under ambient

conditions (Fig. 13A and B). According to the experiments and DFT calculations, the remarkable NRR electrocatalytic performance of the Mo₂C/C composite should primarily be due to the abundant nitrogen adsorption sites of Mo₂C QDs and their particular electronic structure, which contributes to the cleavage and hydrogenation of N≡N bond (Fig. 7C, 13C and D). These studies indicate that MQDs have good prospects in the field of electrocatalysis, but more efforts are still needed for further research.

4.3.2. Photocatalysis. Photocatalysis, another efficient AOP, has been widely researched and has promising potential in handling the global energy and environmental issues.^{5,161–166} MQDs could be excited *via* a broad spectrum ranging from the visible to the NIR, and exhibit attractive surface and electronic properties. Accordingly, MQDs are regarded as promising visible-light catalysts/co-catalysts in photocatalytic CO₂ reduction, H₂ generation, pollutant degradation, and so on. For example, Zeng *et al.*³⁸ developed a hierarchical heterostructure of Ti₃C₂ QD-decorated Cu₂O nanowires (NWs) on a Cu mesh by facile electrostatic self-assembly, for the photocatalytic reduction of CO₂ into methanol. The results showed that the Ti₃C₂ QDs were uniformly anchored on the surface of Cu₂O NWs with intimate contact (Fig. 13E). The methanol production

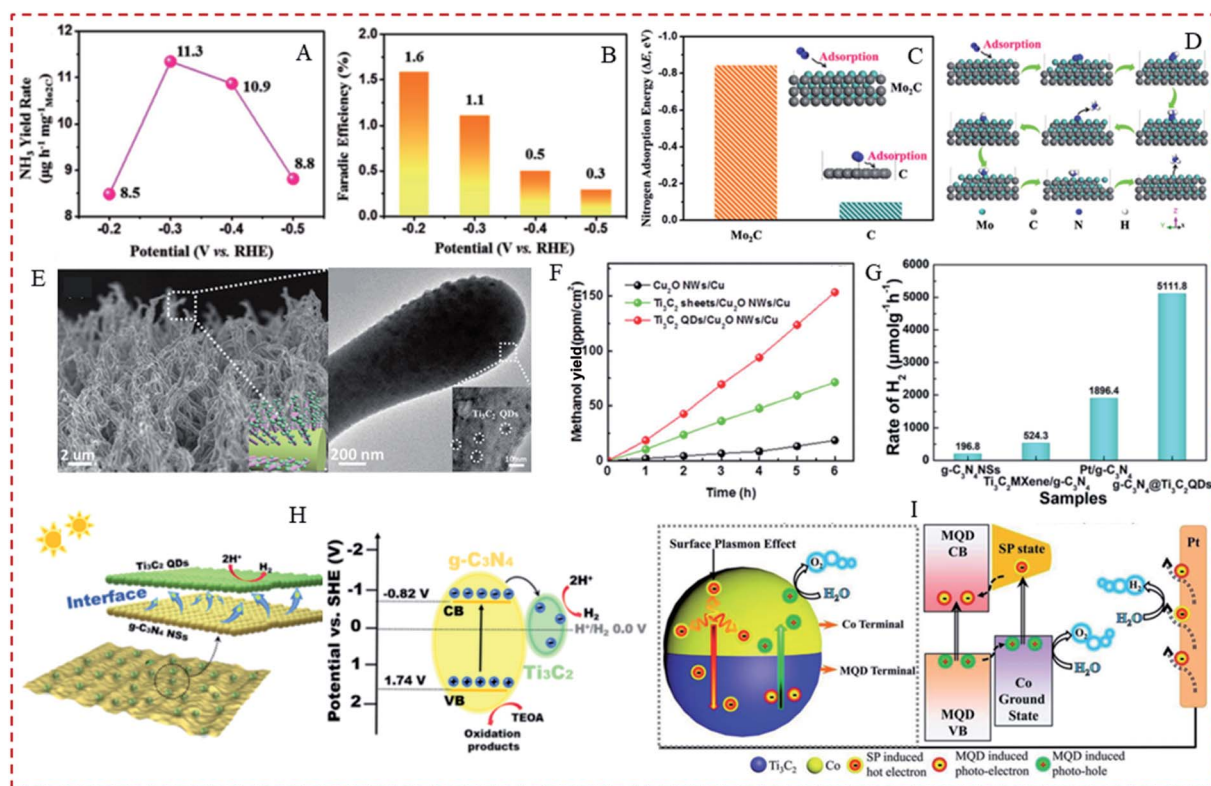


Fig. 13 (A and B) NH₃ synthesis yield rate and corresponding faradaic efficiency.⁷⁰ Copyright 2018 Advanced Materials. (C and D) Nitrogen adsorption energy of Mo₂C QDs and atomistic structure scheme showing the reaction pathway of the N₂ reduction on Mo₂C QD sites.⁷⁰ Copyright 2018 Advanced Materials. (E) SEM and TEM images of Ti₃C₂ QDs on the surface of Cu₂O nanowires.³⁸ Copyright 2019 Advanced Functional Materials. (F) Yields of methanol by the Ti₃C₂ QDs/Cu₂O nanowire composite.³⁸ Copyright 2019 Advanced Functional Materials. (G) Photocatalytic H₂ production rate of g-C₃N₄@Ti₃C₂ QD composites.⁵⁰ Copyright 2019 ACS Applied Materials & Interfaces. (H) Schematic photocatalytic mechanism of g-C₃N₄@Ti₃C₂ QD composites.⁵⁰ Copyright 2019 ACS Applied Materials & Interfaces. (I) Schematic illustration of the light harvesting and carrier separation mechanism of the Janus-structured Co-MQDs.⁶⁰ Copyright 2020 Advanced Functional Materials.

experiment results indicated that the photocatalytic reduction of CO_2 by the Ti_3C_2 QDs/ Cu_2O NWs/ Cu heterostructure was 8.25 or 2.15 times higher than that of Cu_2O NWs/ Cu or Ti_3C_2 sheets/ Cu_2O NWs/ Cu , respectively (Fig. 13F). The significantly improved photocatalytic performance is due to the introduction of Ti_3C_2 QDs, which can enhance charge transfer, carrier density, light adsorption, and the stability of Cu_2O NWs by reducing band bending and photo induced electron-hole pair recombination, and this can be proved by experimental and DFT calculations (Fig. 7B). Li *et al.*⁵⁰ reported that the Ti_3C_2 QDs were successfully combined with $\text{g-C}_3\text{N}_4$ nanosheets as efficient co-catalysts for photocatalytic H_2 generation. The optimized $\text{g-C}_3\text{N}_4$ @ Ti_3C_2 QDs composite (5.5 wt%) could markedly enhance the photocatalytic H_2 production rate ($5111.8 \mu\text{mol g}^{-1} \text{h}^{-1}$), approximately 26, 3, and 10 times higher than the pure $\text{g-C}_3\text{N}_4$ nanosheets ($196.8 \mu\text{mol g}^{-1} \text{h}^{-1}$), $\text{Pt/g-C}_3\text{N}_4$ ($1896.4 \mu\text{mol g}^{-1} \text{h}^{-1}$), and Ti_3C_2 nanosheets/ $\text{g-C}_3\text{N}_4$ ($524.3 \mu\text{mol g}^{-1} \text{h}^{-1}$), respectively (Fig. 13G). The highly efficient photocatalytic performance of the $\text{g-C}_3\text{N}_4$ @ Ti_3C_2 QDs composite can mainly be attributed to the tiny particle size of the Ti_3C_2 QDs co-catalysts, which can increase the specific surface area and provide more active sites. In addition, an intimate contact between metallic Ti_3C_2 QDs and $\text{g-C}_3\text{N}_4$ nanosheets was conducive to transferring photogenerated electrons from $\text{g-C}_3\text{N}_4$ to the conductive Ti_3C_2 QDs. Therefore, the electrons could rapidly participate in the photocatalytic H_2 evolution process (Fig. 13H). These works provide a promising era for the potential application of MQDs in photocatalysis.

4.3.3. Photoelectrocatalysis. Photoelectrocatalysis is a powerful method derived from the combination of heterogeneous photocatalysis and electrochemical techniques. Up to now, there have been some studies regarding the application of 2D MXenes in photoelectrocatalysis for water splitting.^{60,167,168} Therefore, considering the specific character of MQDs, they should also have great application potential in photoelectrocatalysis. In 2020, Tang *et al.*⁶⁰ first reported the study of Ti_3C_2 QDs in photoelectrocatalysis for water oxidation. In this study, a brand-new Janus-structured cobalt-nanoparticle-coupled Ti_3C_2 QD (Co-MQDs) Schottky catalyst was synthesized through a facile thermal-anchoring-hydrothermal method. Coupled with Co terminals, pristine Ti_3C_2 QDs display significantly enhanced water oxidation performance. Remarkably, by virtue of carefully tailoring the heterostructures and Co loading content, the modest Janus-structured Co-MQDs-48 exhibits both superior water oxidation performance (2.99 mA cm^{-2} at 1.23 V vs. RHE) and charge migration efficiency (87.56%). After cycling for 10 h, a photocurrent density of 2.79 mA cm^{-2} could be obtained, confirming the good photostability of Co-MQDs. This outstanding water oxidation performance achieved by Janus-structured Co-MQDs can be attributed to three simultaneous enhancement effects. Firstly, the light harvesting efficiency of pristine Ti_3C_2 QDs can be efficiently improved by Co loading, due to the concomitant surface plasmon effect. Secondly, the carrier separation efficiency of Co-MQDs can be fundamentally enhanced by the Janus-structure introduced Schottky-junction. Thirdly, due to the introduction of the Co terminal, the surface water oxidation performance of

pristine Ti_3C_2 QDs was greatly improved (Fig. 13I). This research provides a new dimension for the application of MQDs in catalysis.

4.4. Energy storage

4.4.1. Batteries. With the progress of science and technology, tremendous attention has been paid to research for developing new-generation electrochemical energy storage technology (such as batteries, supercapacitors and solar cells) and for satisfying the growing requirements of both electronic products and power transmission systems, and the MXene materials have been widely studied in these fields.^{33–35,169,170}

Batteries represent the most extensively studied electrochemical energy storage equipment owing to their environmental friendliness and high energy density.^{14,170,171} In recent years, MXene materials, with superior theoretical Li storage capacity (*e.g.* $447.8 \text{ mA h g}^{-1}$ for Ti_3C_2 and 879 mA h g^{-1} for Mn_2C), favorable electronic conductivity, low operating voltage range, low diffusion barriers for Li mobility (*e.g.* 0.018 eV for Sc_2C), and exceptional mechanical properties, have shown great promise for battery application.^{12,45,96,170} So far, a great deal of research on MXene-based batteries has been reported, in which most of these are 2D MXenes and a few are MQDs. For instance, Xiao *et al.*³⁹ prepared the $\text{Ti}_3\text{C}_2\text{T}_x$ QDs-decorated $\text{Ti}_3\text{C}_2\text{T}_x$ nanosheets/S (TCD-TCS/S) nano-architecture as an electrode for Li-S batteries. The experiment results showed that the TCD-TCS/S electrode exhibited a high discharge capacity (1609 mA h g^{-1}) at a medium sulfur loading of 1.8 mg cm^{-2} . Meanwhile, ultrahigh volumetric capacity ($1957 \text{ mA h cm}^{-3}$) and high areal capacity ($13.7 \text{ mA h cm}^{-2}$) were synchronously achieved at a high sulfur loading of 13.8 mg cm^{-2} . The electrochemical performance was greatly superior to that of traditional carbon-based cathode materials. The mechanistic study of sulfur evolution during the discharge process highlighted the importance of the integration of $\text{Ti}_3\text{C}_2\text{T}_x$ QDs in the Li-S batteries. The uniform interspersed of a high density of ultrafine $\text{Ti}_3\text{C}_2\text{T}_x$ QDs on the surface of the $\text{Ti}_3\text{C}_2\text{T}_x$ nanosheets greatly decreased their interfacial resistance and promoted the redox kinetics of sulfur species, enabling high sulfur utilization even at high current densities and high sulfur loading, thus improving the performance of the batteries significantly (Fig. 14A–C). Zhang *et al.*⁴⁸ employed a simple ball-milling method to prepare a $\text{Ti}_3\text{C}_2\text{T}_x$ QDs/red P composite, and developed it as the anode material for sodium-ion batteries. The results indicated that the composite performed at a high sodiation specific capacity of about 600 mA h g^{-1} at 100 mA g^{-1} , and that it had good cycle stability for 150 cycles. The good performance of this P-based anode can be attributed to the P surface decorated with small $\text{Ti}_3\text{C}_2\text{T}_x$ QDs bound by a strong Ti–O–P interaction, which could improve the robustness of the storage host and its electrical connectivity within the electrode during charge and discharge processes (Fig. 4C, 14D and E). Although there is limited research on MQDs in batteries, these studies indicate that the MQDs could be used as promising electrode material in batteries.

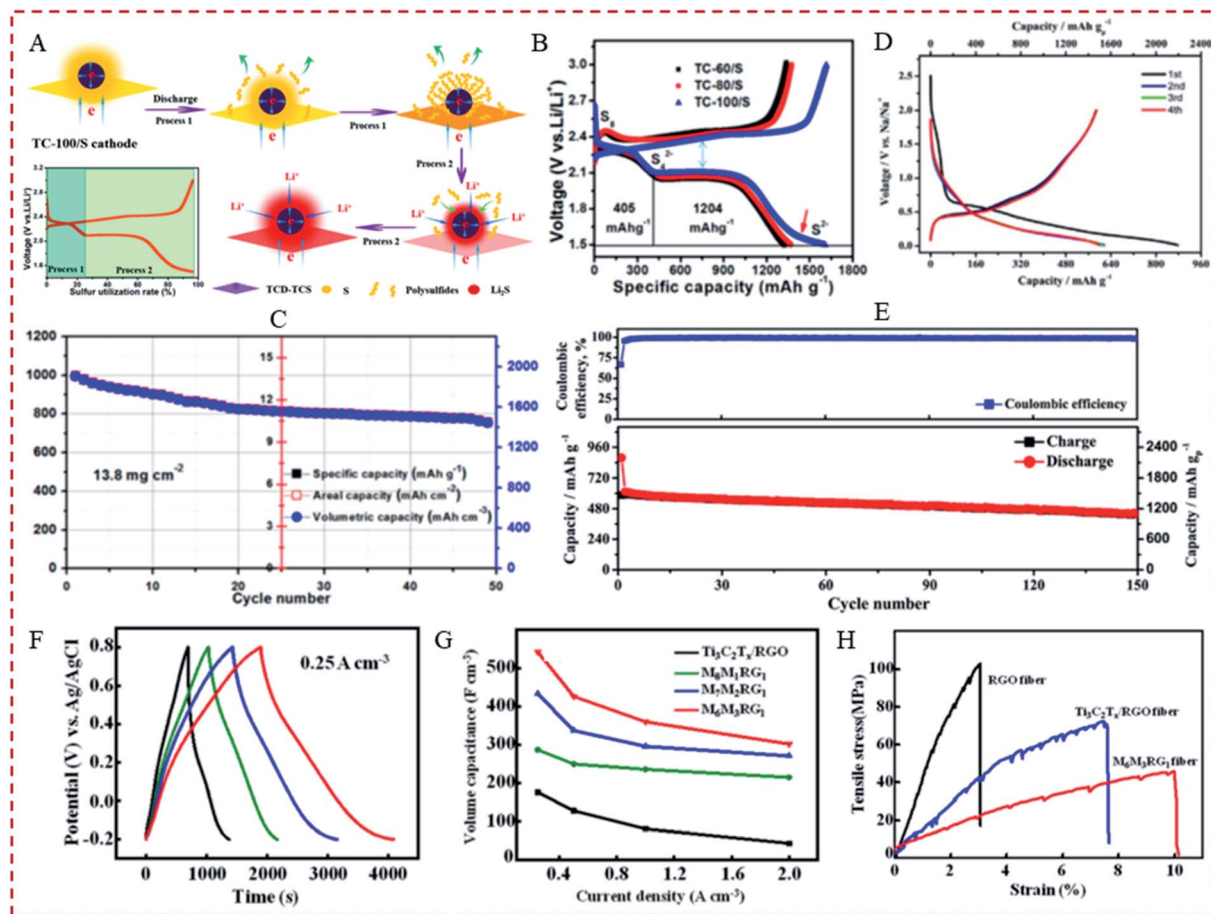


Fig. 14 (A) Schematic illustration for the evolution of active materials during the discharge process for TCD-TCS/S cathodes.³⁹ Copyright 2019 ACS Nano. (B) Voltage profile of the TCD-TCS/S electrodes with an ASL of 1.8 mg cm⁻².³⁹ Copyright 2019 ACS Nano. (C) Cycling performance of TCD-TCS/S electrodes with an ASL of 13.8 mg cm⁻² at 0.05C.³⁹ Copyright 2019 ACS Nano. (D) Galvanostatic charge and discharge curves for the sodium-ion batteries at 100 mA g⁻¹.⁴⁸ Copyright 2018 ChemNanoMat. (E) Cycle stability of the Ti₃C₂T_x QDs/red P composite at 100 mA g⁻¹ as a Na-ion battery anode.⁴⁸ Copyright 2018 ChemNanoMat. Galvanostatic charge-discharge curves (F) and specific capacitance (G) of M_xM_yRG_z obtained with different Ti₃C₂T_x QD amounts.⁶⁴ Copyright 2020 ACS Applied Materials & Interfaces. (H) The mechanical property of the RGO fiber, Ti₃C₂T_x/RGO fiber, and M₆M₃RG₁ fiber.⁶⁴ Copyright 2020 ACS Applied Materials & Interfaces.

4.4.2. Supercapacitors. As well as batteries, a supercapacitor is another vital energy storage device, and is promising to apply in portable electronics and electric vehicles due to the advantages of high power density, rapid charging-discharging ability, and long cycle life.^{172,173} In 2013, Yuri Gogotsi *et al.*¹⁷⁴ first demonstrated that 2D Ti₃C₂T_x could act as flexible and high-performance electrodes in pseudocapacitance. Up to now, 2D MXenes have been widely used in the research of supercapacitors due to their layered 2D structure, good electrical conductivity, hydrophilic surface, flexibility, and highly defined morphology, and this promises to provide rapid electron transfer channels and a large electrochemically active surface for a fast and reversible faradaic reaction, thus giving them ultra-high volumetric capacitance.^{45,169,173,175,176} Although there are limited studies of MQDs in supercapacitors, their great application potential in supercapacitors has also been noticed.⁶⁴ Recently, Zhou *et al.*⁶⁴ reported that Ti₃C₂T_x QDs could be used as interlayer spacers in the positive electrode (Ti₃C₂T_x nanosheets/Ti₃C₂T_x QDs/reduced graphene oxide

(RGO) fiber (M₆M₃RG₁)) of a Ti₃C₂T_x MXene-based all-solid-state asymmetric fiber supercapacitor. In comparison with other interlayer spacers, Ti₃C₂T_x QDs may be selected as good interlayer spacers for the preparation of Ti₃C₂T_x MXene-based fibers, because they not only have a well-defined structure, a conspicuous quantum confinement effect, plentiful edge sites, and abundant functional groups, but they also have the same intrinsic property as Ti₃C₂T_x nanosheets. Therefore, the interactions between the Ti₃C₂T_x nanosheets and Ti₃C₂T_x quantum dots will be kept to a minimum. The experimental results indicated that the network-structured M₆M₃RG₁ fiber electrode possessed an ideal capacitance behavior and a fast charge-discharge performance due to the interlayer spacer function of the Ti₃C₂T_x QDs, and the maximum volumetric capacitance and capacity retention were 542 F cm⁻³ and 56%, respectively. Meanwhile, the capacitance and flexibility are clearly affected by the amount of Ti₃C₂T_x QDs (Fig. 14F–H). This study showed that MQDs could be promising candidates for preparing high-performance supercapacitor materials.

4.5. Optoelectronic devices

Optoelectronics are the key and core components of optoelectronic technology, and with the development of the technology, multifarious optoelectronics are created, including solar cells, light-emitting diodes (LEDs), lasers, and optical switches *etc.*^{177–179} Recent studies have shown that many 2D material derived QDs, such as GQDs, MoS₂ QDs, SiC QDs and MQDs, are outstanding electron acceptors and donors in their photoexcited states, and this makes them promising materials for application in optoelectronics.^{12,61,180} So far, several studies have proved that MQDs could be the ideal materials for white LEDs, white lasers and for nonvolatile memory devices.^{3,47,61,62,72} For example, Xu *et al.*³ developed novel full-color Ti₃C₂ QDs. The prepared Ti₃C₂ QDs showed multi-colors of blue, yellow and orange fluorescence at an excitation of 360 nm. Meanwhile, the acquired Ti₃C₂ QDs have similar PL emission in the solid state,

but the emission experiences red-shifting and PL improvement in aqueous solution, which could be due to the formation of robust bridge-like hydrogen-bonded networks between the Ti₃C₂ QDs and water. The decrease in the band gap due to the π -electron delocalization is responsible for the red-shift of the emissive spectra. Furthermore, the Ti₃C₂ QDs are mixed homogeneously with polyvinylpyrrolidone (PVP) to obtain a white LED, and the LED showed a uniform and stable white light, where the CIE coordinates of (0.31, 0.35) are located near the center of the picture (Fig. 15A and B). Therefore, the full-color Ti₃C₂ QDs are ideal for white LEDs. Huang *et al.*⁷² designed a white laser using V₂C MXene QDs. By passivation, the PL of the V₂C QDs was significantly improved, covering the whole visible region. Under the optimized excitation, the blue, green, yellow, and red lights are amplified and simultaneously lased. Mao *et al.*⁶¹ synthesized an indium tin oxide/Ti₃C₂T_x QDs-

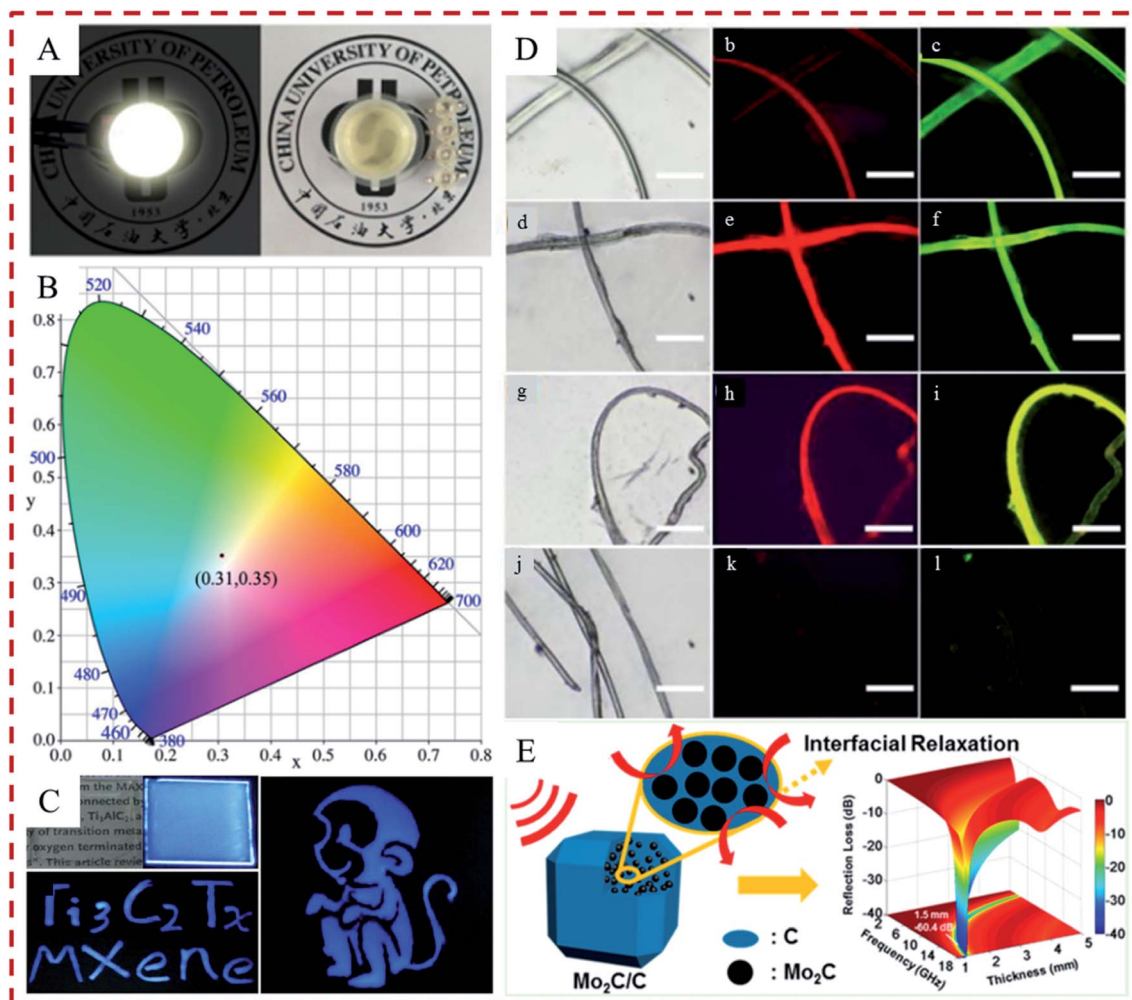


Fig. 15 (A) Fluorescence images of the white Ti₃C₂ QDs/PVP composite under 365 nm emission.³ Copyright 2019 Applied Materials Today. (B) Chromaticity diagram (CIE 1931) coordinates of the white Ti₃C₂ QDs/PVP composite under 360 nm emission (0.31, 0.35).³ Copyright 2019 Applied Materials Today. (C) Photograph of fluorescent words written using the mixture of aqueous GQDs, glycol and PVP as ink, and a printed photograph of a fluorescent "Monkey" pattern under a 365 nm UV lamp.⁴⁷ Copyright 2017 Carbon. (D) Fluorescent images of a silk fiber stained with (a–c) s-Ti₃C₂ QDs, (d–f) e-Ti₃C₂ QDs, (g–i) f-Ti₃C₂ QDs, and (j–l) none, at the excitation wavelengths of (b, e, h, and k) 510–550 nm and (c, f, i, and l) 450–480 nm, respectively.⁴¹ Copyright 2018 Advanced Optical Materials. (E) The microwave absorption performance of the Mo₂C QDs/carbon polyhedrons composite.⁷¹ Copyright 2018 ACS Applied Nano Materials.

PVP/Au (ITO/MQDs-PVP/Au) sandwich structure composite. The results indicated that the electrical conductance of ITO/MQDs-PVP/Au can be tuned precisely from insulator behavior to irreversible resistive switching, reversible resistive switching, and conductor behavior with the increase of $\text{Ti}_3\text{C}_2\text{T}_x$ QDs content. The irreversible and reversible resistive switching behaviors are capable of exhibiting nonvolatile write-once-read-many times and flash memory effects, respectively. Both of the memory devices operate stably under a long retention test (1.2×10^4 s), with a high on/off current ratio of up to 100.

4.6. Other applications

In addition to the above applications, MQDs also exhibited promising application prospects in other fields due to their excellent properties. Zhou *et al.*⁴⁷ reported that $\text{Ti}_3\text{C}_2\text{T}_x$ MXene-derived graphene QDs can be utilized as a fluorescent ink due to their good dispersibility and available PL in various solvents. The experiments indicated that the QDs can be mixed with glycol and polyvinyl pyrrolidone (PVP), and the mixture was colorless under daylight but presented a bright blue color under 365 nm UV illumination, thus it could be immediately applied as fluorescent ink. Meanwhile, the mixture was added into a commercial inkjet printer, and a bright fluorescent “Monkey” picture could be readily printed (Fig. 15C). Xu *et al.*⁴¹ reported that the $\text{Ti}_3\text{C}_2\text{T}_x$ QDs could be used for fluorescent staining of silk fibers. It could be observed that the bright red and green fluorescence could be emitted under different wavelengths after the silk fiber was soaked with $\text{Ti}_3\text{C}_2\text{T}_x$ QDs solution (Fig. 15D). Wang *et al.*⁷¹ found that the Mo_2C QDs could markedly improve the microwave absorption (MA) performance of the $\text{Mo}_2\text{C}/\text{C}$ composite. The improved MA performance can be attributed to the possibility that Mo_2C QDs have an apparent influence on the dielectric loss of the composite, in which conductivity loss and dipole orientation polarization are reasonably decreased, and interfacial polarization is dramatically created, thus improving the impedance matching of the $\text{Mo}_2\text{C}/\text{C}$ composite. The optimal composite had excellent MA performance ranging from 2.0 to 18.0 GHz, including forceful reflection loss (−60.4 dB) and wide qualified bandwidth (14.5 GHz) (Fig. 15E). Although the study on MQDs has been very limited so far, we can predict that they will create enormous attention and be widely studied due to their distinguished optical-electrical and physico-chemical properties.

5. Conclusions and prospects

As an advanced branch of QD materials, MQDs are attracting increasing attention because of their outstanding physico-chemical and optical-electrical properties. The booming progress in exfoliation techniques has promoted the preparation of MQDs with a variety of unique properties, such as excellent PL properties, low toxicity, good biocompatibility and high selectivity to target analytes, and this has created the foundations for the more widespread applications of the MQDs in sensing, bioimaging, cancer therapy, optoelectronics, catalysis and batteries, *etc.* Despite these great achievements, there are still

many fundamental and technical gaps and challenges for this attractive but nascent area.

5.1. Improving synthesis strategies of MQDs

Many studies have shown that there are many ways to synthesize QDs. In the synthesis of MQDs, the top-down method is the most common one, generally, and the 2D MXene precursors were mostly developed by etching the MAX phases in a high concentration acidic solution (such as HF or $\text{LiF} + \text{HCl}$), which is extremely hazardous and detrimental to human health, therefore, it is urgent to explore fluoride-free and environmentally friendly etchants as a sought-after alternative for conventional HF to synthesize the MQDs. Meanwhile, there is little research of bottom-up methods for MQD synthesis. However, some of their advantages, such as higher atomic utilization, better structural control, the feasibility to adjust the dimension and morphology, suggest that this is a promising approach, and should be paid more attention. Furthermore, the stability and monodispersity are particularly important for enhancing the physico-chemical properties and practical applications of MQDs, thus, better methods are needed to be explored. Referring to the synthesis of other QDs, an effective strategy is combining two or more different methods to synthesize more stable and monodisperse MQDs under appropriate conditions. In addition, it is difficult to precisely control the surface chemistry of MQDs, including the preparation of pristine MQDs. The synthesis process is the most direct and convenient process to tune the properties of MQDs for specific applications, thus it is worthwhile to devote more efforts to the synthesis of MQDs.

5.2. Further investigation of the properties of MQDs

MQDs have a variety of important properties because of their unique nanostructures and diverse compositions. Scientists have investigated the physicochemical properties of MQDs mainly by DFT calculations, especially for their electronic and magnetic properties. In experiments, many studies have demonstrated that MQDs possess excellent fluorescence behavior, photothermal conversion, photonic and photoelectronic properties. Although these properties of MQDs have been mentioned, some challenges remain. Efforts are required in the near future to focus on the elucidation of the electron structure-related mechanisms of MQDs to improve their present properties and extend these properties towards new research fields. The combination of theoretical models and practical experiments is an effective approach to explore new MQD nanostructures with new and superior properties. Many properties based on the DFT calculations need to be verified by experiments. Meanwhile, some probable significant properties of MQDs have not been explored, such as up-conversion PL, chemiluminescence and transparent optical properties *etc.* The forthcoming research on MQDs will be rationally driven by the development of other 2D material-derived QDs. The more thoroughly we understand the properties of the MQDs, the easier it is for us to optimize the properties of MQDs. Furthermore, more suitable functionalization measures will be selected

to improve the performance of the MQDs, and this is useful for the improvement of the practical applications of MQDs.

5.3. Functionalized modification of MQDs

The excellent properties of MQDs enable them to have a variety of potential applications, including in biomedical, catalysis, electronic and photoelectronic fields. However, generally, it is difficult to put pristine MQDs into practice due to some inevitable defects. Therefore, prior to these potential applications, MQDs are usually functionalized with other substances or combined with functional materials, and this creates a flexible strategy to overcome these shortcomings and give the MQDs some advantages at the same time, thus increasing the possibility that they can be used in practice. Although some functionalization methods (surface modification, heteroatom doping and constructing composites) have been studied, the research is limited, and more effort is needed to study them further. Noticeably, in different fields, corresponding functionalization strategies should be adopted for the MQDs. For instance, in biological and medical fields, it is better to choose biocompatible materials to act as stabilizing or coating reagents to modify MQDs, such as proteins, peptides and sugars. In the field of catalysis, the MQDs should be immobilized on ideal carriers, thus improving their stability and recyclability. In the optoelectronic and electrochemical devices, the stability, service life, energy conversion efficiency of functionalized MQDs should be especially concerned. When using the modified MQDs for substance detection, it is important to note that the introduced materials during the modification process cannot affect the detection of substances. Therefore, these details should be taken into account in the functionalization processes of MQDs. Furthermore, research on the functionalization of MQDs is still limited, and is mainly focused on surface modification, heteroatom doping and constructing composites. Thus, more effective functionalization methods need to be further studied, such as the core-shell structure MQDs, the immobilized MQDs, *etc.* Synergistic superiority from the MQDs and introduced functional materials will dramatically improve the performance of MQDs, and they will be further developed as good candidates for functionalized nanomaterials in diverse applications by designing versatile and efficient MQD-based intelligent systems.

5.4. Cytotoxicity of MQDs in practical applications

Before practical application, the cytotoxicity of MQDs should be studied, however there are limited studies that have been done up to now. Therefore, to accurately assess the prospective hazards linked to their use and environmental exposure, it is necessary to expand the research of the cytotoxicity of MQDs in practical applications. Like many other QD materials (such as carbon QDs and semiconductor QDs), MQDs are likely to affect living organisms, including animals, plants and microbes, even at low levels, when they are released into the environment. The ultra-small MQDs will cause *in vivo* and *in vitro* cytotoxicity when in contact with living organisms. For *in vivo* cytotoxicity, the MQDs might induce acute toxicity or neurotoxicity at

a certain concentration after the internalization of MQDs into living organisms. For *in vitro* cytotoxicity, the MQDs might cause the canceration or apoptosis of normal cells due to the generation of reactive oxygen species. Furthermore, the surface chemistry of MQDs is an important factor that can affect the potential cytotoxicity, depending on the type of “M” element, the etching and delamination methods, as well as post-functionalization treatment and storage strategies. Therefore, the complicated cytotoxicity of MQDs should be systematically studied, including *in vivo* and *in vitro* cytotoxicity. Meanwhile, the low-cytotoxicity and high-biocompatibility MQDs should be further explored, such as improving their synthesis methods, adjusting their functionalization strategies, and selecting the low-cytotoxicity “M” elements. Only when there is clear understanding of the cytotoxicity of MQDs, can they be applied in practical applications more safely.

5.5. Expanding exploration of diversiform MQDs

Based on classification, MXenes can have at least three different formulas: M_2X , M_3X_2 and M_4X_3 . At the same time, they can be made in three different forms: (i) mono-M elements (*e.g.* Ti_3C_2); (ii) a solid solution of at least two different M elements (*e.g.* $(Ti, V)_3C_2$); (iii) ordered double-M elements, in which one transition metal occupies the perimeter layers and another fills the central M layers (*e.g.* Mo_2TiC_2 , in which the outer M layers are Mo and the central M layers are Ti). Furthermore, solid solutions on the X site produce carbonitride MXenes (*e.g.* Ti_3CN) (Fig. 1C). Among these, over 20 different components of MXenes have been acquired in the experiments, and more than 70 different components of MXenes have been theoretically forecast. The abundant members provide more opportunities to develop diverse MQDs, and the different components of MQDs will endow them with different proprietary properties, allowing them to show extraordinary potential in different areas. However, most research is on Ti_3C_2 QDs so far, and more effort should be paid to other MQDs.

5.6. Enriching the application of MQDs

Although limited research has been done on MQDs until now, their versatile nature has made it possible to apply them in many fields, including in sensing, biomedical applications, catalysis, energy storage, optoelectronic devices *etc.* However, the excellent properties of MQDs signify that their application potential is far from this, and they also show great application potential in some other key technical fields. For example, in solar cell technology, which is a key technology to solving the global energy crisis. So far, a variety of materials have been used in the study of solar cells, but some shortcomings, including the high cost, the low energy efficiency, the short service life, have greatly limited the practical application of solar cells. Meanwhile, many previous studies indicated that the suitable energy band diagram and excellent electronic properties of MXenes have made them become attractive candidates for solar cell applications. Thus, it is well worth spending more efforts to explore the application of MQDs in solar cells. In addition, with the development of intelligent technology, various electronics

have become an indispensable part of modern life. Meanwhile, a future trend in consumer electronics will be the shift towards optically transparent devices. To achieve this, potential primary power sources and related components need to be transparent and resilient. Thus, transparent conducting films will be the key technology to solving this problem, and could be used in the study of batteries, supercapacitors and some other devices to construct optically transparent electronics. Furthermore, with the pollution and exhaustion of fresh water resources, efficient water desalination is becoming an increasingly important means to address the scarcity of fresh water resources in the world, and the nanostructured materials can play an important role in the development of next-generation desalination systems with increased efficiency and capacity. Up to now, there have been many studies on the application of QDs and 2D MXene materials in these fields. However, to the best of our knowledge, there are no reports on the application of MQDs in these fields, and more attention should be paid to study the application of MQDs in these hot research fields. Meanwhile, one thing to note is that although we have only stated the study of the applications of MQDs in these three hot research fields, some other unexplored fields are also worth studying.

Attention must be paid to the above-mentioned issues, as it is of great significance to the development of MQDs. Meanwhile, it is hoped that this review can provide a broad understanding of the range of synthesis, properties and applications of MQDs, and will prompt further developments in these emerging and exciting fields.

Conflicts of interest

There are no conflicts to declare.

Acknowledgements

The study was financially supported by the Program for Changjiang Scholars and Innovative Research Team in University (IRT-13R17), the National Natural Science Foundation of China (51979103, 51679085, 51521006, 51508177, and 51909085), the Fundamental Research Funds for the Central Universities of China (531107050930), and the Funds of Hunan Science and Technology Innovation Project (2018RS3115).

References

- Y. Xu, X. Wang, W. L. Zhang, F. Lv and S. Guo, *Chem. Soc. Rev.*, 2018, **47**, 586–625.
- Q. Xu, W. Cai, W. Li, T. S. Sreeprasad, Z. He, W.-J. Ong and N. Li, *Materials Today Energy*, 2018, **10**, 222–240.
- Q. Xu, W. Yang, Y. Wen, S. Liu, Z. Liu, W.-J. Ong and N. Li, *Applied Materials Today*, 2019, **16**, 90–101.
- J. Hu, D. Chen, Z. Mo, *et al.*, *Angew. Chem., Int. Ed.*, 2019, **58**, 2073–2077.
- B. Shao, X. Liu, Z. Liu, *et al.*, *Chem. Eng. J.*, 2019, **374**, 479–493.
- P. A. Gale, E. N. W. Howe, X. Wu and M. J. Spooner, *Coord. Chem. Rev.*, 2018, **375**, 333–372.
- Y. Wang, M. Qiu, M. Won, E. Jung, T. Fan, N. Xie, S.-G. Chi, H. Zhang and J. S. Kim, *Coord. Chem. Rev.*, 2019, **400**, 213041.
- Y. Liu, D. Huang, M. Cheng, Z. Liu, C. Lai, C. Zhang, C. Zhou, W. Xiong, L. Qin, B. Shao and Q. Liang, *Coord. Chem. Rev.*, 2020, **409**, 213220.
- H. Guo, N. Lu, J. Dai, X. Wu and X. C. Zeng, *J. Phys. Chem. C*, 2014, **118**, 14051–14059.
- Y. Guo, H. Deng, X. Sun, X. Li, J. Zhao, J. Wu, W. Chu, S. Zhang, H. Pan, X. Zheng, X. Wu, C. Jin, C. Wu and Y. Xie, *Adv. Mater.*, 2017, **29**, 1700715.
- C. Chen, M. Boota, P. Urbankowski, B. Anasori, L. Miao, J. Jiang and Y. Gogotsi, *J. Mater. Chem. A*, 2018, **6**, 4617–4622.
- X. Wang, G. Sun, N. Li and P. Chen, *Chem. Soc. Rev.*, 2016, **45**, 2239–2262.
- H. Kim, Z. Wang and H. N. Alshareef, *Nano Energy*, 2019, **60**, 179–197.
- N. K. Chaudhari, H. Jin, B. Kim, D. San Baek, S. H. Joo and K. Lee, *J. Mater. Chem. A*, 2017, **5**, 24564–24579.
- Y. Wang, Y. Liu, J. Zhang, J. Wu, H. Xu, X. Wen, X. Zhang, C. S. Tiwary, W. Yang, R. Vajtai, Y. Zhang, N. Chopra, I. N. Odeh, Y. Wu and P. M. Ajayan, *Sci. Adv.*, 2017, **3**, e1701500.
- R. Gui, H. Jin, Z. Wang and J. Li, *Chem. Soc. Rev.*, 2018, **47**, 6795–6823.
- A. Manikandan, Y.-Z. Chen, C.-C. Shen, C.-W. Sher, H.-C. Kuo and Y.-L. Chueh, *Prog. Quantum Electron.*, 2019, 100226, DOI: 10.1016/j.pquantelec.2019.100226.
- Y. Liu, G. Zeng, H. Zhong, *et al.*, *J. Hazard. Mater.*, 2017, **322**, 394–401.
- B. Anasori, M. R. Lukatskaya and Y. Gogotsi, *Nat. Rev. Mater.*, 2017, **2**, 16098.
- Y. Cao, T. Wu, K. Zhang, X. Meng, W. Dai, D. Wang, H. Dong and X. Zhang, *ACS Nano*, 2019, **13**, 1499–1510.
- T. Niu, *Nano Today*, 2018, **18**, 12–14.
- V. M. Hong Ng, H. Huang, K. Zhou, *et al.*, *J. Mater. Chem. A*, 2017, **5**, 3039–3068.
- M. Naguib, M. Kurtoglu, V. Presser, *et al.*, *Adv. Mater.*, 2011, **23**, 4248–4253.
- F. Bu, M. M. Zagho, Y. Ibrahim, B. Ma, A. Elzatahry and D. Zhao, *Nano Today*, 2019, 100803, DOI: 10.1016/j.nantod.2019.100803.
- J. Zhu, E. Ha, G. Zhao, Y. Zhou, D. Huang, G. Yue, L. Hu, N. Sun, Y. Wang, L. Y. S. Lee, C. Xu, K.-Y. Wong, D. Astruc and P. Zhao, *Coord. Chem. Rev.*, 2017, **352**, 306–327.
- B. Shao, J. Wang, Z. Liu, G. Zeng, L. Tang, Q. Liang, Q. He, T. Wu, Y. Liu and X. Yuan, *J. Mater. Chem. A*, 2020, **8**, 5171–5185.
- J. Peng, X. Chen, W.-J. Ong, *et al.*, *Chem*, 2019, **5**, 18–50.
- H. Wang, Y. Wu, X. Yuan, G. Zeng, J. Zhou, X. Wang and J. W. Chew, *Adv. Mater.*, 2018, **30**, 1704561.
- D. Sun, Q. Hu, J. Chen, X. Zhang, L. Wang, Q. Wu and A. Zhou, *ACS Appl. Mater. Interfaces*, 2016, **8**, 74–81.
- M. Naguib, O. Mashtalir, J. Carle, V. Presser, J. Lu, L. Hultman, Y. Gogotsi and M. W. Barsoum, *ACS Nano*, 2012, **6**, 1322–1331.

- 31 B. Anasori, A. Sarycheva, S. Buondonno, Z. Zhou, S. Yang and Y. Gogotsi, *Mater. Today*, 2017, **20**, 481–482.
- 32 J. Pang, R. G. Mendes, A. Bachmatiuk, L. Zhao, H. Q. Ta, T. Gemming, H. Liu, Z. Liu and M. H. Rummeli, *Chem. Soc. Rev.*, 2019, **48**, 72–133.
- 33 A. Agresti, A. Pazniak, S. Pescetelli, A. Di Vito, D. Rossi, A. Pecchia, M. Auf der Maur, A. Liedl, R. Larciprete, D. V. Kuznetsov, D. Saranin and A. Di Carlo, *Nat. Mater.*, 2019, **18**, 1228–1234.
- 34 L. Yu, A. S. R. Bati, T. S. L. Grace, M. Batmunkh and J. G. Shapter, *Adv. Energy Mater.*, 2019, **9**, 1901063.
- 35 L. Yang, Y. Dall'Agnese, K. Hantanasirisakul, C. E. Shuck, K. Maleski, M. Alhabeb, G. Chen, Y. Gao, Y. Sanehira, A. K. Jena, L. Shen, C. Dall'Agnese, X.-F. Wang, Y. Gogotsi and T. Miyasaka, *J. Mater. Chem. A*, 2019, **7**, 5635–5642.
- 36 Z. Guo, L. Gao, Z. Xu, S. Teo, C. Zhang, Y. Kamata, S. Hayase and T. Ma, *Small*, 2018, **14**, 1802738.
- 37 Q. Xue, H. Zhang, M. Zhu, Z. Pei, H. Li, Z. Wang, Y. Huang, Y. Huang, Q. Deng, J. Zhou, S. Du, Q. Huang and C. Zhi, *Adv. Mater.*, 2017, **29**, 1604847.
- 38 Z. Zeng, Y. Yan, J. Chen, *et al.*, *Adv. Funct. Mater.*, 2019, **29**, 1806500.
- 39 Z. Xiao, Z. Li, P. Li, X. Meng and R. Wang, *ACS Nano*, 2019, **13**, 3608–3617.
- 40 A. Rafieerad, W. Yan, G. L. Sequiera, N. Sareen, E. Abu-El-Rub, M. Moudgil and S. Dhingra, *Adv. Healthcare Mater.*, 2019, **8**, e1900569.
- 41 G. Xu, Y. Niu, X. Yang, Z. Jin, Y. Wang, Y. Xu and H. Niu, *Adv. Opt. Mater.*, 2018, **6**, 1800951.
- 42 M. Khazaei, A. Mishra, N. S. Venkataramanan, A. K. Singh and S. Yunoki, *Curr. Opin. Solid State Mater. Sci.*, 2019, **23**, 164–178.
- 43 K. Huang, Z. Li, J. Lin, G. Han and P. Huang, *Chem. Soc. Rev.*, 2018, **47**, 5109–5124.
- 44 K. Rasool, R. P. Pandey, P. A. Rasheed, S. Buczek, Y. Gogotsi and K. A. Mahmoud, *Mater. Today*, 2019, **30**, 80–102.
- 45 H. Wang, Y. Wu, X. Yuan, G. Zeng, J. Zhou, X. Wang and J. W. Chew, *Adv. Mater.*, 2018, **30**, e1704561.
- 46 X. Yu, X. Cai, H. Cui, S. W. Lee, X. F. Yu and B. Liu, *Nanoscale*, 2017, **9**, 17859–17864.
- 47 L. Zhou, F. Wu, J. Yu, Q. Deng, F. Zhang and G. Wang, *Carbon*, 2017, **118**, 50–57.
- 48 T. Zhang, X. Jiang, G. Li, Q. Yao and J. Y. Lee, *ChemNanoMat*, 2018, **4**, 56–60.
- 49 X. Chen, X. Sun, W. Xu, G. Pan, D. Zhou, J. Zhu, H. Wang, X. Bai, B. Dong and H. Song, *Nanoscale*, 2018, **10**, 1111–1118.
- 50 Y. Li, L. Ding, Y. Guo, Z. Liang, H. Cui and J. Tian, *ACS Appl. Mater. Interfaces*, 2019, **11**, 41440–41447.
- 51 Z. Guo, X. Zhu, S. Wang, C. Lei, Y. Huang, Z. Nie and S. Yao, *Nanoscale*, 2018, **10**, 19579–19585.
- 52 M. Liu, J. Zhou, Y. He, Z. Cai, Y. Ge, J. Zhou and G. Song, *Microchim. Acta*, 2019, **186**, 770.
- 53 X. Xu, H. Zhang, Q. Diao, Y. Zhu and B. Ma, *J. Mater. Sci.: Mater. Electron.*, 2019, **31**, 175–181.
- 54 Y. Qin, Z. Wang, N. Liu, Y. Sun, D. Han, Y. Liu, L. Niu and Z. Kang, *Nanoscale*, 2018, **10**, 14000–14004.
- 55 Y. Feng, F. Zhou, Q. Deng and C. Peng, *Ceram. Int.*, 2020, **46**, 8320–8327.
- 56 Q. Xu, L. Ding, Y. Wen, W. Yang, H. Zhou, X. Chen, J. Street, A. Zhou, W.-J. Ong and N. Li, *J. Mater. Chem. C*, 2018, **6**, 6360–6369.
- 57 Q. Guan, J. Ma, W. Yang, R. Zhang, X. Zhang, X. Dong, Y. Fan, L. Cai, Y. Cao, Y. Zhang, N. Li and Q. Xu, *Nanoscale*, 2019, **11**, 14123–14133.
- 58 X. Yang, Q. Jia, F. Duan, B. Hu, M. Wang, L. He, Y. Song and Z. Zhang, *Appl. Surf. Sci.*, 2019, **464**, 78–87.
- 59 M. Liu, Y. He, J. Zhou, Y. Ge, J. Zhou and G. Song, *Anal. Chim. Acta*, 2020, **1103**, 134–142.
- 60 R. Tang, S. Zhou, C. Li, R. Chen, L. Zhang, Z. Zhang and L. Yin, *Adv. Funct. Mater.*, 2020, 2000637.
- 61 H. Mao, C. Gu, S. Yan, Q. Xin, S. Cheng, P. Tan, X. Wang, F. Xiu, X. Liu, J. Liu, W. Huang and L. Sun, *Adv. Electron. Mater.*, 2020, **6**, 1900493.
- 62 S. Lu, L. Sui, Y. Liu, X. Yong, G. Xiao, K. Yuan, Z. Liu, B. Liu, B. Zou and B. Yang, *Adv. Sci.*, 2019, **6**, 1801470.
- 63 M. L. Desai, H. Basu, R. K. Singhal, S. Saha and S. K. Kailasa, *Colloids Surf., A*, 2019, **565**, 70–77.
- 64 X. Zhou, Y. Qin, X. He, Q. Li, J. Sun, Z. Lei and Z.-H. Liu, *ACS Appl. Mater. Interfaces*, 2020, **12**, 11833–11842.
- 65 X. Chen, J. Li, G. Pan, W. Xu, J. Zhu, D. Zhou, D. Li, C. Chen, G. Lu and H. Song, *Sens. Actuators, B*, 2019, **289**, 131–137.
- 66 G. Cai, Z. Yu, P. Tong and D. Tang, *Nanoscale*, 2019, **11**, 15659–15667.
- 67 Z. Wang, J. Xuan, Z. Zhao, Q. Li and F. Geng, *ACS Nano*, 2017, **11**, 11559–11565.
- 68 Q. Zhang, Y. Sun, M. Liu and Y. Liu, *Nanoscale*, 2020, **12**, 1826–1832.
- 69 W. Dai, H. Dong and X. Zhang, *Materials*, 2018, **11**, 1776.
- 70 H. Cheng, L. X. Ding, G. F. Chen, L. Zhang, J. Xue and H. Wang, *Adv. Mater.*, 2018, **30**, e1803694.
- 71 Y. Wang, C. Li, X. Han, D. Liu, H. Zhao, Z. Li, P. Xu and Y. Du, *ACS Appl. Nano Mater.*, 2018, **1**, 5366–5376.
- 72 D. Huang, Y. Xie, D. Lu, Z. Wang, J. Wang, H. Yu and H. Zhang, *Adv. Mater.*, 2019, **31**, e1901117.
- 73 G. Yang, J. Zhao, S. Yi, X. Wan and J. Tang, *Sens. Actuators, B*, 2020, **309**, 127735.
- 74 X. Li, M. Rui, J. Song, Z. Shen and H. Zeng, *Adv. Funct. Mater.*, 2015, **25**, 4929–4947.
- 75 R. Feng, W. Lei, X. Sui, X. Liu, X. Qi, K. Tang, G. Liu and M. Liu, *Appl. Catal., B*, 2018, **238**, 444–453.
- 76 G. Li, Z. Lian, W. Wang, D. Zhang and H. Li, *Nano Energy*, 2016, **19**, 446–454.
- 77 S. Xu, D. Li and P. Wu, *Adv. Funct. Mater.*, 2015, **25**, 1127–1136.
- 78 L.-L. Li, J. Ji, R. Fei, C.-Z. Wang, Q. Lu, J.-R. Zhang, L.-P. Jiang and J.-J. Zhu, *Adv. Funct. Mater.*, 2012, **22**, 2971–2979.
- 79 Y. Xu, Z. Wang, Z. Guo, H. Huang, Q. Xiao, H. Zhang and X.-F. Yu, *Adv. Opt. Mater.*, 2016, **4**, 1223–1229.
- 80 Q. Liang, X. Liu, G. Zeng, *et al.*, *Chem. Eng. J.*, 2019, **372**, 429–451.
- 81 R. Tomita, Y. Yasu, T. Koike and M. Akita, *Angew. Chem., Int. Ed.*, 2014, **53**, 7144–7148.

- 82 M.-C. Chang and S.-A. Chen, *J. Polym. Sci., Part A: Polym. Chem.*, 1987, **25**, 2543–2559.
- 83 M. Malaki, A. Maleki and R. S. Varma, *J. Mater. Chem. A*, 2019, **7**, 10843–10857.
- 84 H. Xu, B. W. Zeiger and K. S. Suslick, *Chem. Soc. Rev.*, 2013, **42**, 2555–2567.
- 85 M. Bromberger Soquetta, S. Schmaltz, F. Wesz Righes, R. Salvalaggio and L. de Marsillac Terra, *J. Food Process. Preserv.*, 2018, **42**, e13393.
- 86 D. Gopalakrishnan, D. Damien, B. Li, H. Gullappalli, V. K. Pillai, P. M. Ajayan and M. M. Shaijumon, *Chem. Commun.*, 2015, **51**, 6293–6296.
- 87 K. Jiang, Y. Wang, X. Gao, C. Cai and H. Lin, *Angew. Chem., Int. Ed.*, 2018, **57**, 6216–6220.
- 88 L. Lei, D. Huang, G. Zeng, M. Cheng, D. Jiang, C. Zhou, S. Chen and W. Wang, *Coord. Chem. Rev.*, 2019, **399**, 213020.
- 89 M. Khazaei, M. Arai, T. Sasaki, C.-Y. Chung, N. S. Venkataramanan, M. Estili, Y. Sakka and Y. Kawazoe, *Adv. Funct. Mater.*, 2013, **23**, 2185–2192.
- 90 X. Zhang, J. Lei, D. Wu, *et al.*, *J. Mater. Chem. A*, 2016, **4**, 4871–4876.
- 91 R. Lotfi, M. Naguib, D. E. Yilmaz, J. Nanda and A. C. T. van Duin, *J. Mater. Chem. A*, 2018, **6**, 12733–12743.
- 92 J.-C. Lei, X. Zhang and Z. Zhou, *Frontiers of Physics*, 2015, **10**, 276–286.
- 93 K. Hantanasirisakul and Y. Gogotsi, *Adv. Mater.*, 2018, **30**, 1804779.
- 94 M. Khazaei, A. Ranjbar, M. Arai, T. Sasaki and S. Yunoki, *J. Mater. Chem. C*, 2017, **5**, 2488–2503.
- 95 B.-M. Jun, S. Kim, J. Heo, C. M. Park, N. Her, M. Jang, Y. Huang, J. Han and Y. Yoon, *Nano Res.*, 2018, **12**, 471–487.
- 96 X. Zhang, Z. Zhang and Z. Zhou, *J. Energy Chem.*, 2018, **27**, 73–85.
- 97 P. Zhao, Q. Xu, J. Tao, Z. Jin, Y. Pan, C. Yu and Z. Yu, *Wiley Interdiscip. Rev.: Nanomed. Nanobiotechnol.*, 2018, **10**, e1483.
- 98 R. M. Ronchi, J. T. Arantes and S. F. Santos, *Ceram. Int.*, 2019, **45**, 18167–18188.
- 99 P. Chakraborty, T. Das and T. Saha-Dasgupta, *Compr. Nanosci. Nanotechnol.*, 2019, 319–330, DOI: 10.1016/b978-0-12-803581-8.10414-x.
- 100 B. Anasori, C. Shi, E. J. Moon, Y. Xie, C. A. Voigt, P. R. C. Kent, S. J. May, S. J. L. Billinge, M. W. Barsoum and Y. Gogotsi, *Nanoscale Horiz.*, 2016, **1**, 227–234.
- 101 M. Khazaei, M. Arai, T. Sasaki, M. Estili and Y. Sakka, *Phys. Chem. Chem. Phys.*, 2014, **16**, 7841–7849.
- 102 M. Khazaei, M. Arai, T. Sasaki, A. Ranjbar, Y. Liang and S. Yunoki, *Phys. Rev. B: Condens. Matter Mater. Phys.*, 2015, **92**, 075411.
- 103 M. Khazaei, A. Ranjbar, M. Arai and S. Yunoki, *Phys. Rev. B*, 2016, **94**, 125152.
- 104 Y. Liang, M. Khazaei, A. Ranjbar, M. Arai, S. Yunoki, Y. Kawazoe, H. Weng and Z. Fang, *Phys. Rev. B*, 2017, **96**, 195414.
- 105 C. Si, K.-H. Jin, J. Zhou, Z. Sun and F. Liu, *Nano Lett.*, 2016, **16**, 6584–6591.
- 106 S. Zhu, Y. Song, J. Wang, H. Wan, Y. Zhang, Y. Ning and B. Yang, *Nano Today*, 2017, **13**, 10–14.
- 107 R. Li, L. Zhang, L. Shi and P. Wang, *ACS Nano*, 2017, **11**, 3752–3759.
- 108 Z. Guo, J. Zhou, L. Zhu and Z. Sun, *J. Mater. Chem. A*, 2016, **4**, 11446–11452.
- 109 H. Ding, S.-B. Yu, J.-S. Wei and H.-M. Xiong, *ACS Nano*, 2016, **10**, 484–491.
- 110 L. Zhang, L. Yin, C. Wang, N. lun, Y. Qi and D. Xiang, *J. Phys. Chem. C*, 2010, **114**, 9651–9658.
- 111 Y. Xu, J. Liu, C. Gao and E. Wang, *Electrochem. Commun.*, 2014, **48**, 151–154.
- 112 Z. Ling, C. E. Ren, M.-Q. Zhao, J. Yang, J. M. Giammarco, J. Qiu, M. W. Barsoum and Y. Gogotsi, *Proc. Natl. Acad. Sci. U. S. A.*, 2014, **111**, 16676–16681.
- 113 Z. Gan, X. Wu, G. Zhou, J. Shen and P. K. Chu, *Adv. Opt. Mater.*, 2013, **1**, 554–558.
- 114 N. Mauser, D. Piatkowski, T. Mancabelli, M. Nyk, S. Mackowski and A. Hartschuh, *ACS Nano*, 2015, **9**, 3617–3626.
- 115 C. Zhang, B. Anasori, A. Seral-Ascaso, S.-H. Park, N. McEvoy, A. Shmeliov, G. S. Duesberg, J. N. Coleman, Y. Gogotsi and V. Nicolosi, *Adv. Mater.*, 2017, **29**, 1702678.
- 116 S. Kim, J. Kim, D. Kim, B. Kim, H. Chae, H. Yi and B. Hwang, *ACS Appl. Mater. Interfaces*, 2019, **11**, 26333–26338.
- 117 K. Hantanasirisakul, M.-Q. Zhao, P. Urbankowski, J. Halim, B. Anasori, S. Kota, C. E. Ren, M. W. Barsoum and Y. Gogotsi, *Adv. Electron. Mater.*, 2016, **2**, 1600050.
- 118 P. Salles, E. Quain, N. Kurra, A. Sarycheva and Y. Gogotsi, *Small*, 2018, **14**, 1802864.
- 119 G. Deysher, S. Sin, Y. Gogotsi and B. Anasori, *Mater. Today*, 2018, **21**, 1064–1065.
- 120 J. Li, X. Yuan, C. Lin, Y. Yang, L. Xu, X. Du, J. Xie, J. Lin and J. Sun, *Adv. Energy Mater.*, 2017, **7**, 1602725.
- 121 S. Lai, J. Jeon, S. K. Jang, J. Xu, Y. J. Choi, J.-H. Park, E. Hwang and S. Lee, *Nanoscale*, 2015, **7**, 19390–19396.
- 122 Y. Liu, M. Cheng, Z. Liu, *et al.*, *Chemosphere*, 2019, **236**, 124387.
- 123 X. Wang, G. Sun, P. Routh, D.-H. Kim, W. Huang and P. Chen, *Chem. Soc. Rev.*, 2014, **43**, 7067–7098.
- 124 J. P. Paraknowitsch and A. Thomas, *Energy Environ. Sci.*, 2013, **6**, 2839–2855.
- 125 Z. Liu, B. Shao, G. Zeng, *et al.*, *Chemosphere*, 2018, **210**, 922–930.
- 126 Y. Jiang, Z. Liu, G. Zeng, Y. Liu, B. Shao, Z. Li, Y. Liu, W. Zhang and Q. He, *Environ. Sci. Pollut. Res.*, 2018, **25**, 6158–6174.
- 127 Y. Liu, Z. Liu, G. Zeng, *et al.*, *J. Hazard. Mater.*, 2018, **357**, 10–18.
- 128 B. Shao, Z. Liu, H. Zhong, *et al.*, *Microbiol. Res.*, 2017, **200**, 33–44.
- 129 R. Gusain, N. Kumar and S. S. Ray, *Coord. Chem. Rev.*, 2020, **405**, 213111.
- 130 H. Zhong, Z. Wang, Z. Liu, Y. Liu and M. Yu, *Int. Biodeterior. Biodegrad.*, 2016, **115**, 141–145.

- 131 Z. Wang, C. Xu, Y. Lu, X. Chen, H. Yuan, G. Wei, G. Ye and J. Chen, *Sens. Actuators, B*, 2017, **241**, 1324–1330.
- 132 W. Kong, Y. Niu, M. Liu, K. Zhang, G. Xu, Y. Wang, X. Wang, Y. Xu and J. Li, *Inorg. Chem. Commun.*, 2019, **105**, 151–157.
- 133 J. Liu, G. Lv, W. Gu, Z. Li, A. Tang and L. Mei, *J. Mater. Chem. C*, 2017, **5**, 5024–5030.
- 134 H. Zhong, H. Zhang, Z. Liu, X. Yang, M. L. Brusseau and G. Zeng, *Sci. Rep.*, 2016, **6**, 33266.
- 135 W. Zhang, Z. Zeng, Z. Liu, J. Huang, R. Xiao, B. Shao, Y. Liu, Y. Liu, W. Tang, G. Zeng, J. Gong and Q. He, *Ecotoxicol. Environ. Saf.*, 2020, **189**, 109914.
- 136 R. Bilan, I. Nabiev and A. Sukhanova, *ChemBioChem*, 2016, **17**, 2103–2114.
- 137 C. H. R, J. D. Schiffman and R. G. Balakrishna, *Sens. Actuators, B*, 2018, **258**, 1191–1214.
- 138 A. Sinha, Dhanjai, H. Zhao, Y. Huang, X. Lu, J. Chen and R. Jain, *TrAC, Trends Anal. Chem.*, 2018, **105**, 424–435.
- 139 P. A. Gale and C. Caltagirone, *Coord. Chem. Rev.*, 2018, **354**, 2–27.
- 140 R. Gui, H. Jin, X. Bu, Y. Fu, Z. Wang and Q. Liu, *Coord. Chem. Rev.*, 2019, **383**, 82–103.
- 141 Z. Liang, M. Kang, G. F. Payne, X. Wang and R. Sun, *ACS Appl. Mater. Interfaces*, 2016, **8**, 17478–17488.
- 142 F. Zu, F. Yan, Z. Bai, J. Xu, Y. Wang, Y. Huang and X. Zhou, *Microchim. Acta*, 2017, **184**, 1899–1914.
- 143 B. Shao, Z. Liu, G. Zeng, *et al.*, *J. Hazard. Mater.*, 2019, **362**, 318–326.
- 144 X. Wu, E. N. W. Howe and P. A. Gale, *Acc. Chem. Res.*, 2018, **51**, 1870–1879.
- 145 E. N. W. Howe and P. A. Gale, *J. Am. Chem. Soc.*, 2019, **141**, 10654–10660.
- 146 Z. Peng, X. Liu, W. Zhang, *et al.*, *Environ. Int.*, 2020, **134**, 105298.
- 147 S. Cheung, D. Wu, H. C. Daly, N. Busschaert, M. Morgunova, J. C. Simpson, D. Scholz, P. A. Gale and D. F. O'Shea, *Chem*, 2018, **4**, 879–895.
- 148 S. Filali, F. Pirot and P. Miossec, *Trends Biotechnol.*, 2020, **38**, 163–177.
- 149 K.-T. Yong, W.-C. Law, R. Hu, L. Ye, L. Liu, M. T. Swihart and P. N. Prasad, *Chem. Soc. Rev.*, 2013, **42**, 1236–1250.
- 150 H. Lin, S. Gao, C. Dai, Y. Chen and J. Shi, *J. Am. Chem. Soc.*, 2017, **139**, 16235–16247.
- 151 A. Zhang, A. Li, W. Zhao and J. Liu, *Chem.–Eur. J.*, 2018, **24**, 4215–4227.
- 152 Y. Chen, Y. Wu, B. Sun, S. Liu and H. Liu, *Small*, 2017, **13**, 1603446.
- 153 V. P. Shastri and A. Lendlein, *Adv. Mater.*, 2009, **21**, 3231–3234.
- 154 X. Hao, Z. Jin, H. Yang, G. Lu and Y. Bi, *Appl. Catal., B*, 2017, **210**, 45–56.
- 155 L. Kong, Y. Ji, Z. Dang, J. Yan, P. Li, Y. Li and S. Liu, *Adv. Funct. Mater.*, 2018, **28**, 1800668.
- 156 X. Qian, D. Yue, Z. Tian, M. Reng, Y. Zhu, M. Kan, T. Zhang and Y. Zhao, *Appl. Catal., B*, 2016, **193**, 16–21.
- 157 S. Wu, H. Li, X. Li, H. He and C. Yang, *Chem. Eng. J.*, 2018, **353**, 533–541.
- 158 T. Wu, X. Liu, Y. Liu, *et al.*, *Coord. Chem. Rev.*, 2020, **403**, 213097.
- 159 S.-J. Li, D. Bao, M.-M. Shi, B.-R. Wulan, J.-M. Yan and Q. Jiang, *Adv. Mater.*, 2017, **29**, 1700001.
- 160 B. Huang, N. Li, W.-J. Ong and N. Zhou, *J. Mater. Chem. A*, 2019, **7**, 27620–27631.
- 161 B. Shao, X. Liu, Z. Liu, *et al.*, *Chem. Eng. J.*, 2019, **368**, 730–745.
- 162 B. Shao, Z. Liu, G. Zeng, *et al.*, *ACS Sustainable Chem. Eng.*, 2018, **6**, 16424–16436.
- 163 L. Jiang, X. Yuan, G. Zeng, J. Liang, Z. Wu, H. Wang, J. Zhang, T. Xiong and H. Li, *Environ. Sci.: Nano*, 2018, **5**, 2604–2617.
- 164 Z. Liu, Y. Jiang, X. Liu, G. Zeng, B. Shao, Y. Liu, Y. Liu, W. Zhang, W. Zhang, M. Yan and X. He, *Composites, Part B*, 2019, **173**, 106918.
- 165 Y. Liu, Z. Liu, D. Huang, M. Cheng, G. Zeng, C. Lai, C. Zhang, C. Zhou, W. Wang, D. Jiang, H. Wang and B. Shao, *Coord. Chem. Rev.*, 2019, **388**, 63–78.
- 166 Y. Pan, X. Liu, W. Zhang, Z. Liu, G. Zeng, B. Shao, Q. Liang, Q. He, X. Yuan, D. Huang and M. Chen, *Appl. Catal., B*, 2020, **265**, 118579.
- 167 J. Lin, Y. Yu, Z. Zhang, F. Gao, S. Liu, W. Wang and G. Li, *Adv. Funct. Mater.*, 2020, **30**, 1910479.
- 168 X. Yu, T. Wang, W. Yin and Y. Zhang, *Int. J. Hydrogen Energy*, 2019, **44**, 2704–2710.
- 169 C. Zhan, M. Naguib, M. Lukatskaya, P. R. C. Kent, Y. Gogotsi and D.-e. Jiang, *J. Phys. Chem. Lett.*, 2018, **9**, 1223–1228.
- 170 Z. Xiao, Z. Li, X. Meng and R. Wang, *J. Mater. Chem. A*, 2019, **7**, 22730–22743.
- 171 N. K. Chaudhari, H. Jin, B. Kim and K. Lee, *Nanoscale*, 2017, **9**, 12231–12247.
- 172 Q. Li, Y. Chen, J. Zhang, W. Tian, L. Wang, Z. Ren, X. Ren, X. Li, B. Gao, X. Peng, P. K. Chu and K. Huo, *Nano Energy*, 2018, **51**, 128–136.
- 173 A. S. Levitt, M. Alhabeab, C. B. Hatter, A. Sarycheva, G. Dion and Y. Gogotsi, *J. Mater. Chem. A*, 2019, **7**, 269–277.
- 174 M. R. Lukatskaya, O. Mashtalir, C. E. Ren, Y. Dall'Agnese, P. Rozier, P. L. Taberna, M. Naguib, P. Simon, M. W. Barsoum and Y. Gogotsi, *Science*, 2013, **341**, 1502.
- 175 Q. Jiang, N. Kurra, M. Alhabeab, Y. Gogotsi and H. N. Alshareef, *Adv. Energy Mater.*, 2018, **8**, 1703043.
- 176 M. Ghidui, M. R. Lukatskaya, M.-Q. Zhao, Y. Gogotsi and M. W. Barsoum, *Nature*, 2014, **516**, 78–81.
- 177 A. P. Litvin, I. V. Martynenko, F. Purcell-Milton, A. V. Baranov, A. V. Fedorov and Y. K. Gun'ko, *J. Mater. Chem. A*, 2017, **5**, 13252–13275.
- 178 H. V. Demir, S. Nizamoglu, T. Erdem, E. Mutlugun, N. Gaponik and A. Eychmüller, *Nano Today*, 2011, **6**, 632–647.
- 179 H. Zhao, J. Xia, D. Yin, M. Luo, C. Yan and Y. Du, *Coord. Chem. Rev.*, 2019, **390**, 32–49.
- 180 S. C. Dhanabalan, B. Dhanabalan, J. S. Ponraj, Q. Bao and H. Zhang, *Adv. Opt. Mater.*, 2017, **5**, 1700257.